ULTRA-VIOLET DEGRADATION BEHAVIOR OF POLYMERIC BACKSHEETS FOR PHOTOVOLTAIC MODULES

A Thesis
Submitted to the Graduate Faculty
of the
North Dakota State University
of Agriculture and Applied Science

By

Fei Liu

In Partial Fulfillment of the Requirements
for the Degree of
MASTER OF SCIENCE

Major Department:
Mechanical Engineering

October 2013

Fargo, North Dakota

North Dakota State University
Graduate School

Title

Ultra-Violet Degradation Behavior of Polymeric Backsheets for Photovoltaic Modules

By

Fei Liu

The Supervisory Committee certifies that this ***disquisition*** complies with North Dakota State University's regulations and meets the accepted standards for the degree of

MASTER OF SCIENCE

SUPERVISORY COMMITTEE:

Dr. Long Jiang
Chair

Dr. Chad Ulven

Dr. Dilpreet Bajwa

Dr. Dennis Wiesenborn

Dr. Shuying Yang

Approved:

1/17/2014
Date

Dr. Alan Kallmeyer
Department Chair

ABSTRACT

This study is designed to understand the ultra-violet (UV) degradation of polymeric backsheets used in PV modules. Commercial photovoltaic backsheets from four suppliers were UV-aged for up to 3000 hours. The aged samples were tested using optical microscopy, scanning electron microscopy (SEM), shrinkage rate test, color measurements, UV-Vis-NIR, Fourier transform infrared spectroscopy (FTIR), and dielectrical tests to study the microstructural, color, chemical and electrical properties. Yellowness Index (YI) and Delta E were used to quantify the color changes which were found in strong correlation with FTIR results. The characters of the surface cracks generated were found to be affected by degree of UV degradation and polymer chain alignment of the backsheets. Electrical properties were not significantly affected by UV irradiation. The results suggest insufficient UV aging time designated in current PV module test standard. A longer aging time is recommended for quality assurance.

ACKNOWLEDGEMENT

I would like to thank my advisor Dr. Long Jiang for his great help, support, patience and guidance not only during the development and completion of this thesis project, but also through the entire journey of my graduate program. Dr. Shuying Yang, Senior Staff Engineer at MEMC/SunEdison, made a great contribution to this thesis. My supervisory committee members Dr. Chad Ulven, Dr. Dennis Wiesenborn and Dr. Dilpreet Bajwa also offered great help in the development of this thesis. I am also grateful to the help on the part of Scanning Electronic Microscopy provided by Scott Payne and Jayma Moore in NDSU Electron Microscopy Center. The help on the testing of color change and UV-vis-NIR from Instrumental Laboratory Manager, Heidi Docktor in NDSU's Department of Coatings and Polymeric Materials is deeply appreciated. Dr. Haagenson Darrin is sincerely appreciated for his instruction on Fourier Transform Infrared Spectroscopy. Last but not least, my group members of Xuezhu Xu, Yong Wang, David Gutschmidt are also deeply appreciated during the preparation of the thesis defense.

TABLE OF CONTENTS

LIST OF TABLES

LIST OF FIGURES

CHAPTER 1. INTRODUCTION AND LITERATURE REVIEW

1.1. Solar Energy and Solar Panel (Structure, Materials, and Theory)

Renewable energy has attracted intensive research interest over the past decade. Solar energy is one of the most competitive forms of renewable energy resources. On average, 1.2×10^{17} W of solar irradiation is received by the Earth[1]. This abundant and environment-friendly energy can be converted directly into electricity using solar photovoltaic (PV) technology, which has experienced dramatic technological advancement and market growth in recent years.[2]

Since the invention of the silicon PV cells in Bell Laboratories,[3] PV system (single-junction) has reached a theoretical efficiency of about 25%, though the practical efficiency being much lower (about 15%).[4] Although the operation of a PV system requires no or minimum energy consumption and low maintenance, the initial investment is high. This feature demands long service life of the PV system to lower its life cycle cost. Current standard warranty of PV modules typically ranges from 25 to 30 years. Thus, a thorough understanding of the aging/durability of the PV modules and their subcomponents is of critical importance to achieve their long term stable performance.

1.1.1. Terminology Definition

The conversion of solar light into electricity by photovoltaic effect of semiconductors is called solar photovoltaics. A single PV convertor cell is called a solar cell or a PV cell (Fig.

1); a combination of such cells designed to increase the electronic power output is a solar module/panel.[5] Electrical contacts are on the front and back side of a PV cell, bridging the semiconductor material and the external electrical load. The back contact simply consists of a layer of aluminum or molybdenum, while the front contact is a grid of metal strips or "fingers". Busbars are used to collect the electrons from the fingers.[6]

Fig. 1. Photo of an actual PV cell. The horizontal lines are the fingers and the two vertical ones are the busbars.[7]

1.1.2. Working Principle of PV

A PV process is based on the ability of semiconductors to convert solar energy into electricity. Generally, when light is shone onto the surface of a semiconductor material, the energy of photons would be absorbed and transferred to electrons. When the energy absorbed passes a threshold, it is sufficient to liberate the electrons from the constraint of the atoms. Then, electron-hole pairs are created and free to move along circuits to generate electrical current (Fig. 2).

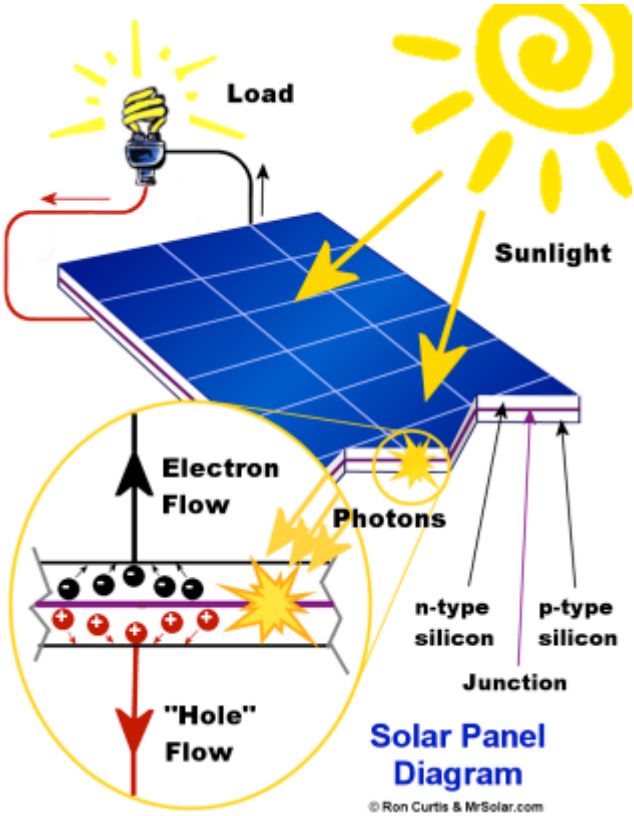

Fig. 2. Illustration of the working principal of a solar panel.[8]

1.1.3. Classification

PV cells can be made from different semiconducting materials, including crystalline silicon (single-crystal silicon, polycrystalline/multicrystalline silicon, etc.), amorphous silicon (a-Si), gallium arsenide (GaAs), and copper indium diselenide (CuInSe2, or CIS), etc. Depending on how solar irradiation is collected, PV systems can be classified into two major categories: flat plate photovoltaic (FPV) system, in which the solar cells receive solar irradiation directly; and concentrating photovoltaic (CPV) system, in which solar irradiation is collected and concentrated to the solar cells.

NREL (National Renewable Energy Lab) keeps track of the efficiency of the different PV cells. Fig. 3 presents the developments of PV technologies over the past 4 decades.

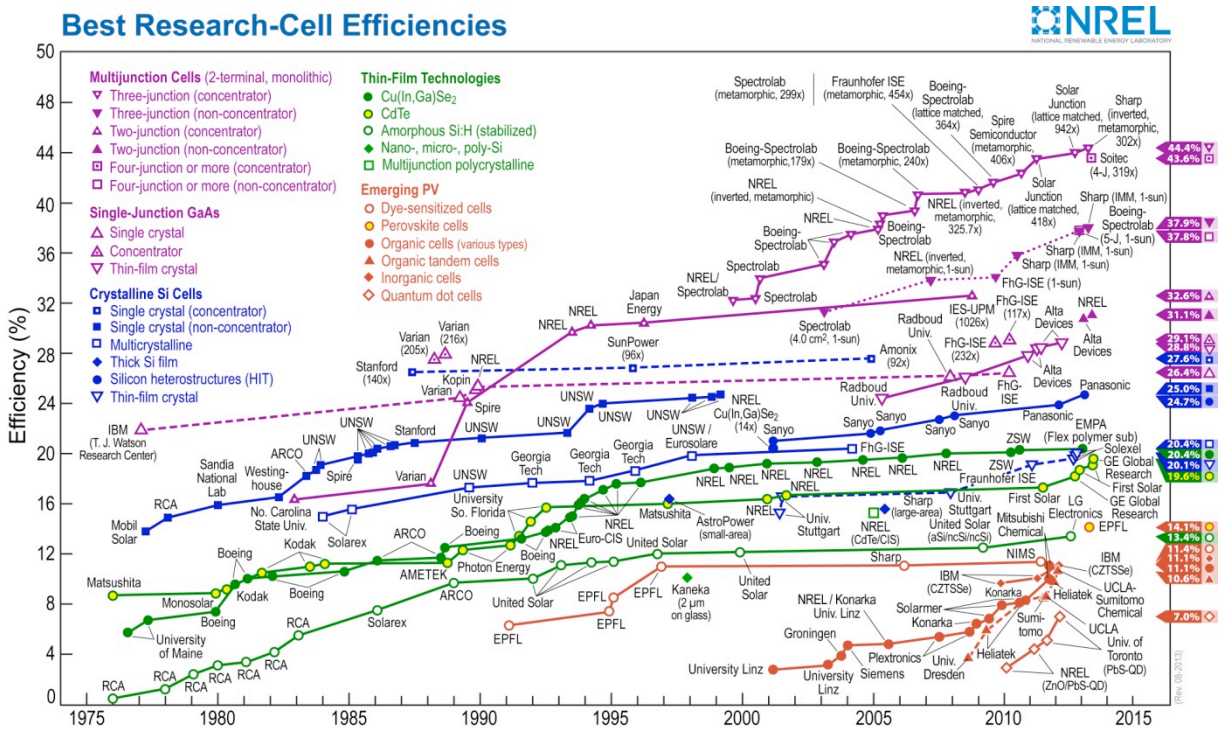

Fig. 3. Efficiency improvements of various types of PV cells.[9]

1.1.4. Solar Module Structure

To ensure a PV module's long service life, PV cells have to be encapsulated and sealed in a package to protect them from rapid environmental degradation caused by oxidation from the contacts of metals, ultraviolet light, temperature, moisture and mechanical stresses. In addition to the encapsulants in direct contact with the PV cells, polymeric backsheet materials are also commonly used in PV modules for physical protection, enhanced encapsulation, light reflection, electrical insulation and aesthetic purposes.

Typical structures of a crystalline silicon solar cell are shown in Fig. 4 and Fig. 5. Generally, the laminate structure consists of five layers: front glass, front EVA encapsulant, PV cells, back EVA encapsulant, and backsheet (or backfoil).

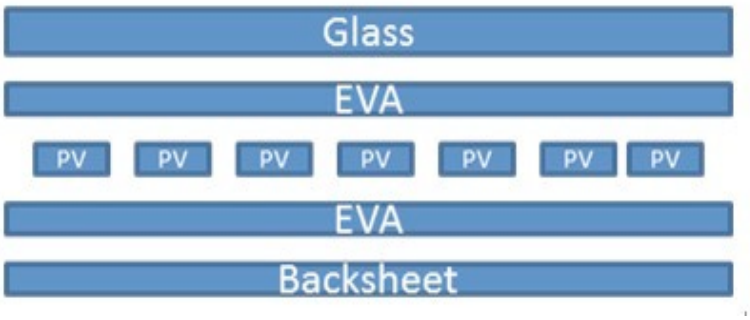

Fig. 4. Typical laminate structure of a PV module. Polymers other than EVA can also be used as encapsulants in PV modules.[10]

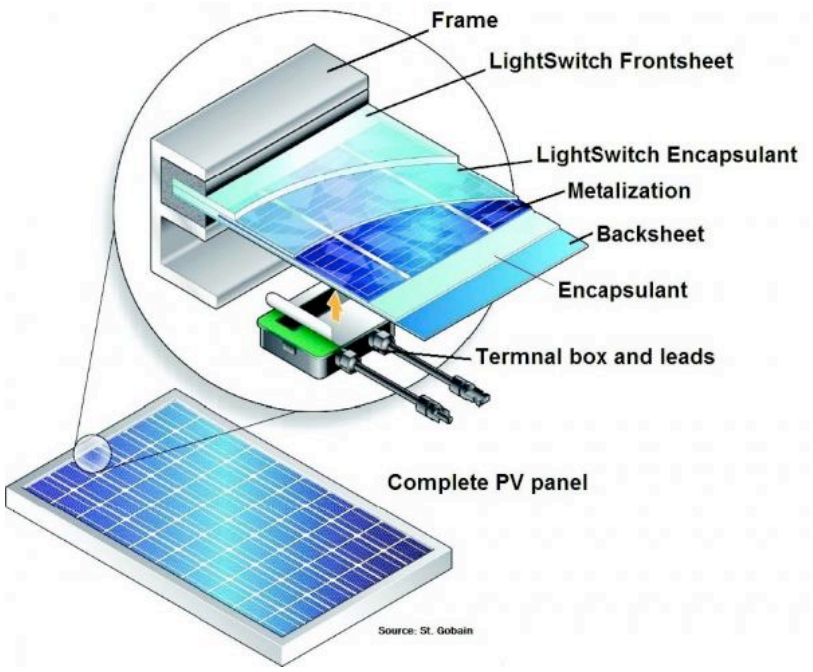

Fig. 5. Illustration of the structure of a PV panel/module.[11]

Materials other than EVA, including thermoplastic polyurethane (TPU), polyvinyl butyral (PVB), silicones, silicone/PU hybrid, ionomer, UV-curable resin, and other new polymers, can also be used as the encapsulants for PV modules. EVA is the most widely used material due to its low cost and long service history.

For the front glass (or the superstrate), low-iron, tempered, plain or textured, UV filtering Ce-glass, SiO_2, or antireflection coating glass can be used. Transparent fluoropolymers, such as Tefzel® and Tedlar®, have also been applied as alternatives to glass.

For the backsheets, a variety of materials and substructures are used, including Tedlar® based polymers and polyethylene terephthalate (PET) or polyethylene naphthalate (PEN) based polymers. The Tedkar® based backsheets include: Tedlar®/PET/Tedlar® (TPT), Tedlar®/PET/EVA (TPE), Tedlar®/Al foil/EVA (TAT), Tedlar®/PET/Al foil/Tedlar® (TPAT), Tedlar®/PET/Oxide/Tedlar® (TPOT), and PEN/Al foil/PET (PAP). PET or PEN based backsheets provide less expensive alternatives to Tedlar®. Among this type of materials are Protekt® and Teijin Teonex ®. Sometimes glass is also used to replace polymer backsheets.[12]

The main factors influencing the aging of PV modules include:

- Corrosion of metal materials
- Delamination of encapsulant polymers
- Physical damage from environmental weather elements, such as wind, sand, rain, snow, and hail
- Damage from shipping and installation
- Deterioration of external components, such as wiring and frames
- Erosion from permeated water vapor
- Thermal process
- Ultraviolet (UV) irradiation.[13]

Among these factors the last three are the most important ones which cause severe PV module degradation. The polymers in a PV module, including EVA encapsulants, backsheet

and junction boxes, are known to have inadequate weatherabilities.[14] Thus their durability is critical to the long term performance of solar panels.

1.2. Field Failures and Quality Testing

Accelerated tests are often used to identify potential failure mechanisms in PV modules and to estimate the rate of their occurrences in the real systems.

1.2.1. Failures of Solar Panels

Under continuous environmental stresses the components of solar panels are prone to malfunctions and failures after long term service. Typical field failures of a PV module include:

- Cracks in the glass or within the cells/films
- Significant visual changes on either the active side or back side of a module such as cracking, color changes (Fig. 6 and Fig. 7), or delamination (Fig. 8)
- Electrical short circuits or burned spots
- Obvious corrosion of lead or cell interconnections
- Significant distortions in the module shape, including frame distortion and flatness
- Power lead failures, including separation from junction box or connectors and cracking of insulation
- Junction box changes, including separation from the module, and movement along the backsheet. (Fig. 9)

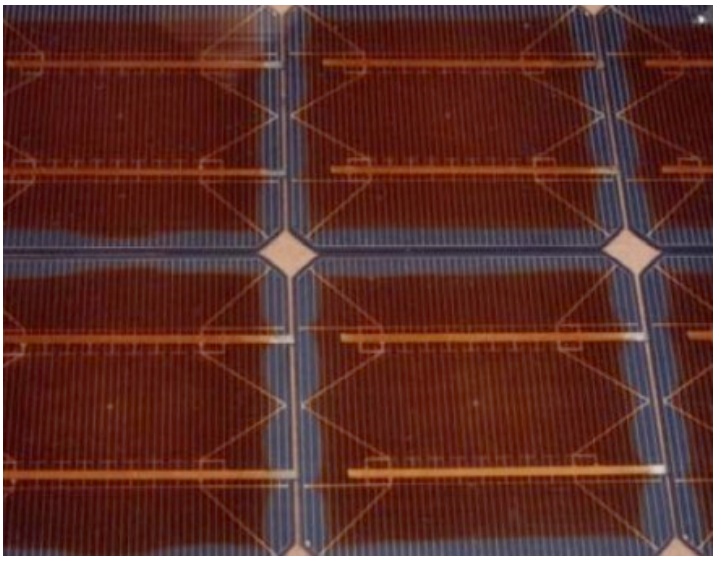

Fig. 6. Significant browning of the front encapsulant of PV modules, where most likely the polymeric encapsulant has insufficient UV stability.[12]

Fig. 7. Typical backsheet yellowing after short period of field installation.[15]

Fig. 8. Delamination of the backsheet of a PV module.[12]

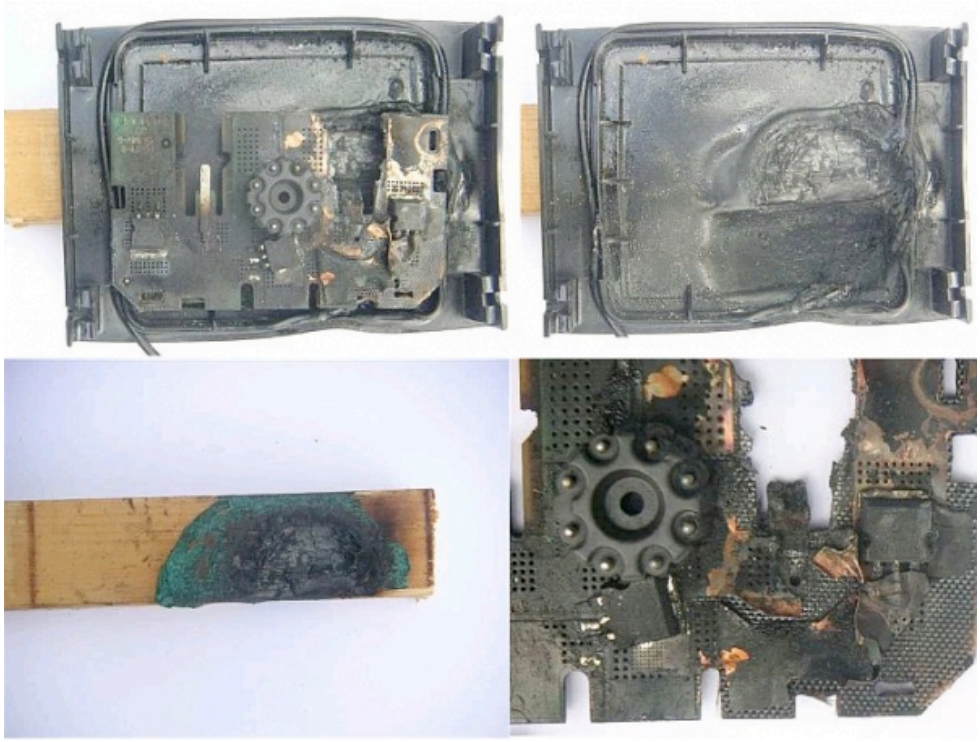

Fig. 9. Junction box failures.[16]

A summary of PV module failures is given in Table 1. Almost all the failures in the table lead to safety risks and reduced performance. Therefore, their mechanisms need to be thoroughly studied and the methods for improvement need to be developed.

Table 1. Principal failure modes in PV modules.[17]

Defects and failure	Component	Seriousness for performance	Seriousness for safety	Stresses
Delamination	Glass and Encapsulant	H		UV, T, H, Ion
	Encapsulant and cells	H		
	Encapsulant and backsheet		M	
	Inter-layer of backsheet		M	
Discoloration	Encapsulant	M		UV, T, H, Material design
	Backsheet			
Backsheet cracking, decomposition	Backsheet	M	M	UV, T, H

1.2.2. Importance of Backsheets

PV modules are supposed to be a reliable source of power for at least 25 years, so the components need to work in concert to ensure the panel continues to perform. Backsheets help do that – they insulate the electrical components of the module to ensure they can operate safely and protect them over their service life to help modules produce power efficiently. The functions of backsheets include:

- Physical protection
- Moisture protection
- Durability
- Electrical insulation
- Color that helps modules blend into their surroundings
- Efficiency to help modules generate more power

PV module manufacturers use different components and constructions. Selecting the right backsheet for a specific module design is often complex, and time-consuming.[18]

1.2.3. Certification Standards

To ensure long term service of solar panels in the field, the International Electrotechnical Commission (IEC) has established qualification test standard (IEC 61215 for crystalline silicon flat PV modules). The flow chart of the IEC 61215 standard is shown in Fig. 10. The standard regulates the testing in diagnostic, electrical, performance, thermal, irradiance, environmental, and mechanical areas. For outdoor exposure test, the required irradiation is 60 kWh/m^2, which is far short compared to the irradiation received by a module within its 25 to 30 years of service.

The International PV Module Quality Assurance (QA) Task Force[19] led by NREL is working to address the quality assurance issues of the PV modules through interdisciplinary studies and collaborative projects among a wide range of stakeholders (PV manufacturers, test labs, standards organizations, customers, investors, etc.). The goal of the PV QA Task Force is to create standards that allow the stakeholders to quickly assess a module's ability to withstand regional stresses, thereby reducing risk and adding confidence for those developing products, designing incentive programs, and determining investments and bankability assessment.

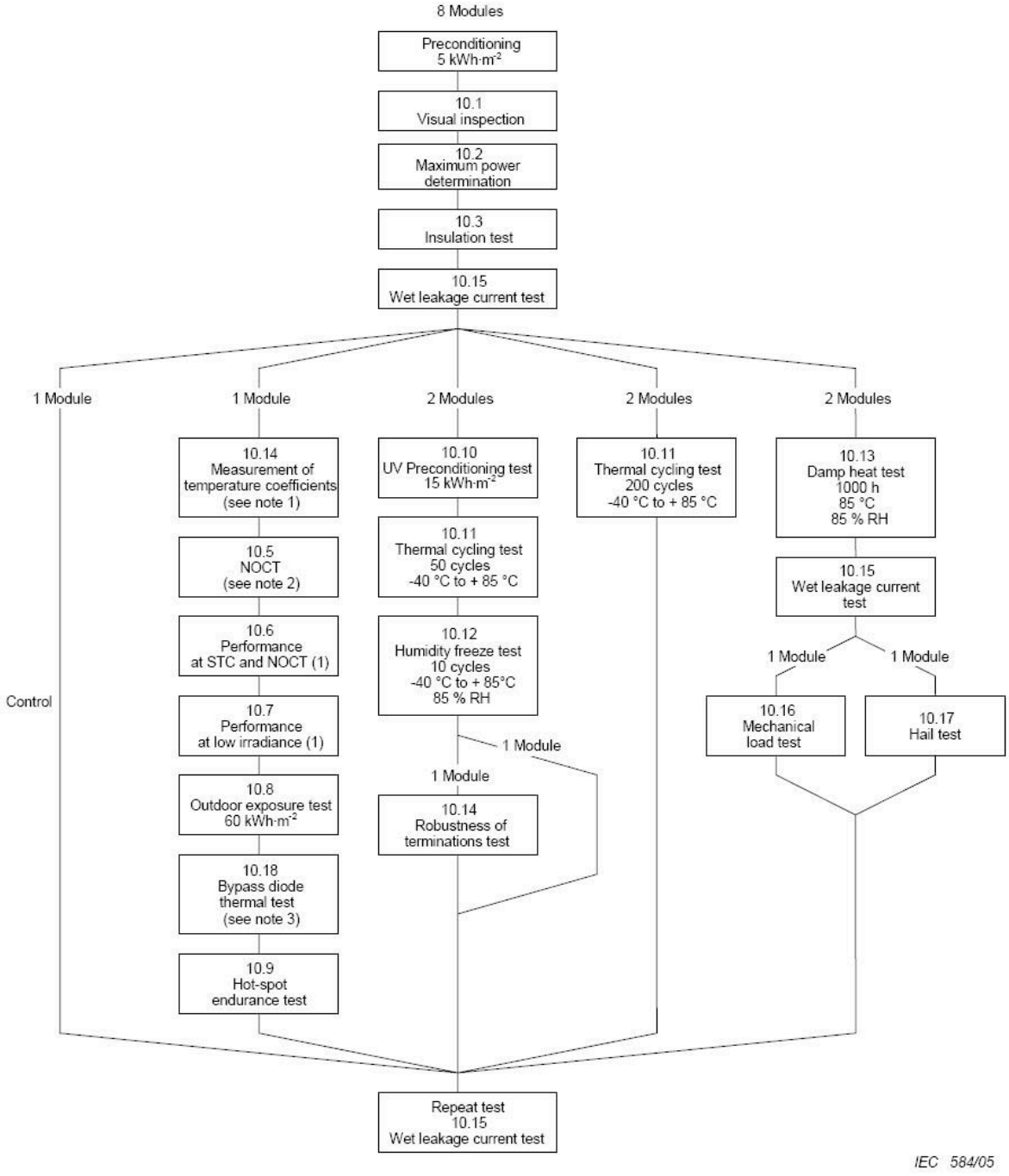

Fig. 10. Flow chart of IEC 61215 testing process.[20]

The PV QA Task Force includes the following Task Groups:

- Group 1: Guideline for manufacturing consistency

- Group 2: Testing for thermal and mechanical fatigue including vibration
- Group 3: Testing for humidity, temperature, and voltage
- Group 4: Testing for diodes, shading and reverse bias
- Group 5: Testing for UV, temperature and humidity
- Group 6: Communication of PV QA ratings to the community
- Group 7: Testing for wind loading
- Group 8: Testing for thin-film PV
- Group 9: Testing for CPV

This research is part of a bigger project of Task Group 5. Basically, the responsibilities of this group include testing and understanding the aging behavior of PV packaging materials under UV, sunlight, temperature, moisture level, etc.

Current qualification test standards of PV modules lay down IEC requirements for the design qualification and type approval[20], describe the fundamental construction requirements[21] for general PV modules, and cover requirements for flat-plate PV modules and panels[22] and concentrator photovoltaic (CPV) modules and assemblies[23]. IEC 61215[20] and IEC 61646[24] specify a short-term UV preconditioning test, with a UV dosage of 15 kWh/m^2 for indoor exposure testing, and 60 kWh/m^2 for outdoor exposure testing, comparing to in-field annual dosage on the order of 100 kWh/m^2 and lifetime (25 years) dosage of 3000 kWh/m^2.[25] This preconditioning test is carried out in order to identify materials that are susceptible to UV degradation before the thermal cycle and humidity freeze tests are performed. However, the PV module qualification test standards do not provide information about simulation of outdoor exposure under UV irradiation for the lifetime of PV modules.

Accelerated tests under field conditions are difficult to carry out because parameters that can be accelerated are limited. Accelerated lifetime tests require enhanced UV power than sunlight, higher temperature than practical situation, and the neglecting of dark periods without sunlight irradiation that cannot be avoided in practical applications. Their combination with humidity as a potential reagent in the module degradation processes makes the tests even more challenging.

The tests used in this thesis falls between qualification testing and accelerated testing. Qualification testing applies indoor tests to acquire quick information of the quality, while accelerated testing simulates field conditions to obtain data for the service life time. The test-to-failure protocol extends the artificial indoor stresses by perform the testing until the failures of modules. The time lengths of the tests do not indicate the service life time of a module. However, they can be compared quantitatively to indicate the stability of modules.

1.2.4. Current Testing Methods for Light Aging

Current methods for light aging include indoor/chamber testing and outdoor testing. In indoor/chamber testing three light sources[26], including metal halide arc, UV fluorescence and Xenon arc, are commonly used to age the specimens. Typical spectra of the three light sources are provided in Fig. 11, Fig. 12 and Fig. 13. Metal halide light contains a wide range of spectrum and causes fast material aging. However, it may introduce artificial degradation. Fluorescence UV light produces a fairly good match to the UV from natural sunlight. Commercial fluorescence UV equipment is easy to operate. However, it does not contain visible light spectrum. Xenon arc generates light that closely matches the full spectrum of natural sunlight. However, only 1X sun intensity is available from commercial equipment. The intensity of the light can be elevated to different multiples of that of the natural sunlight

to perform accelerated aging tests. In outdoor testing, samples are mounted in fields and are exposed to 1X intensity of sunlight. In Equatorial Mount with Mirrors for Acceleration with Water (EMMAQUA) testing, sunlight is concentrated by mirrors and samples are exposed to 4X to 5X concentrated sunlight. It provides an excellent match to sunlight in subtropical areas and desert environment, such as Arizona.[27]

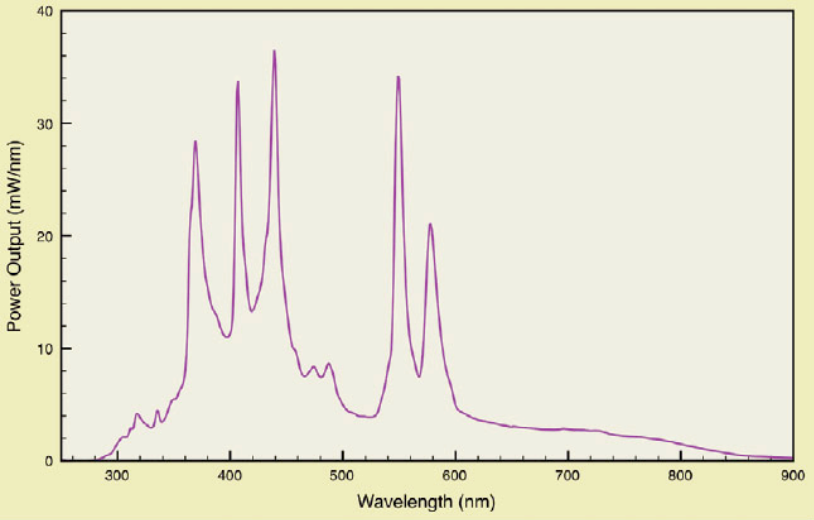

Fig. 11. Spectrum of a typical metal halide arc lamp.[28]

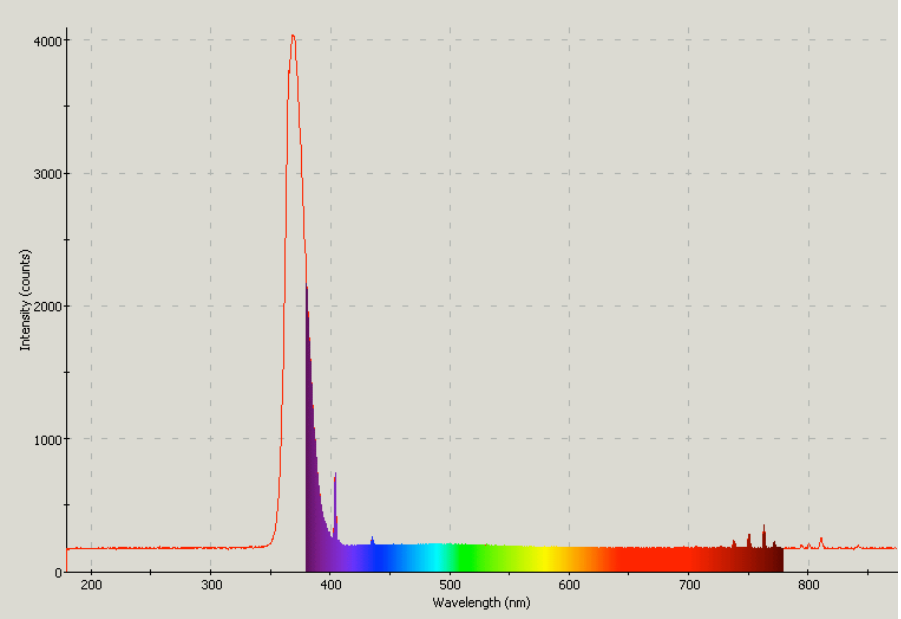

Fig. 12. Spectrum from a portable UVA (long wave UV) fluorescent lamp.[29]

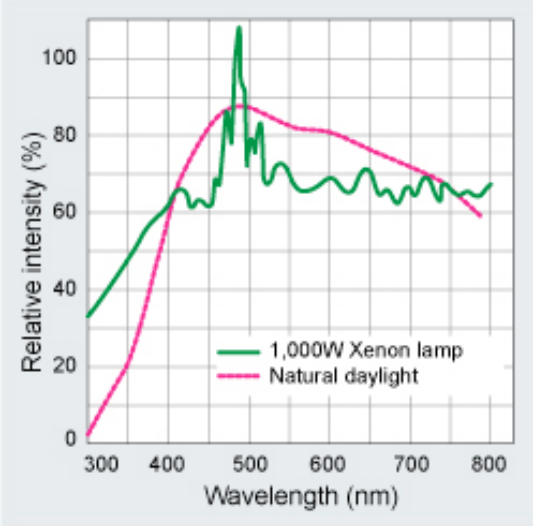

Fig. 13. Spectrum comparison between a xenon lamp and natural daylight.[30]

1.2.5. Yellowing and Yellowness Index (YI)

Yellowing is one of the serious failures of PV backsheets after long-term irradiation. The yellow color is usually caused by the formation of chromophores (sections of macromolecular

chains that selectively absorb different frequencies of visible light, lending colors to the molecules). Serious backsheet yellowing has resulted in customer claims to some solar module products.[31]

Yellowness Index is a critical parameter for monitoring degradation of the encapsulant materials and backsheets because higher yellowness leads to higher absorption of irradiation and thus higher operating temperature (which in return accelerates the degradation process) and lower energy absorption by the PV cells (which results in lower electricity production). The procedures to measure YI are specified in ASTM E313.[32] Generally, YI is calculated by using this equation:

$$YI=100(C_X X-C_Z Z)/Y \quad (1)$$

where X, Y, and Z are the International Commission on Illumination (CIE) tristimulus values of the sample and can be obtained using color measuring instruments. C_x and C_z are two coefficients that can be selected from ASTM E313[32] based on the operating standard of the color measuring instruments. YI test is intended to provide values correlated with visual estimates under specified observing conditions[32]. Due to the subjectivity of visual estimates and the variety of visual observing condition, spectrophotometers need to be used to produce accurate YI results.

1.2.6. Accelerated Tests on PV Module Parts

Two major concerns about PV module quality assurance are: How long will a PV module remain operational? And can accelerated tests provide answers to this question within relatively short period of experiment time? Many studies have been performed to develop standard testing methods to address these two concerns. In a typical accelerated test, samples

undergo aging process under elevated UV irradiation, temperature and humidity stresses in weathering chambers for 3–4 months. This type of tests has been widely used in PV product development.

Focusing on UV degradation, a typical accelerated UV irradiation test is performed continuously without night intervals. As high as 42 times the intensity of sunlight can be applied and simulation data for as long as decades can be calculated from only thousands of hours of tests.[33]

However, C. R. Osterwald *et al.*[13] reviewed the literature about accelerated stress testing of PV modules from 1975 to 2008 and deemed that the standard tests and procedures that had been established so far were not rigorous enough to determine the service life of PV cells because they did not apply all the failure mechanisms.

Backsheets are critical components in a PV module and their UV aging behavior plays a pivotal role in long-term PV module function and performance. A typical backsheet structure includes three layers of polymer films laminated together, with or without adhesives in between. The common inner layer material is EVA or LDPE. The middle layer is often made of PET for mechanical strength and electrical insulation and the outer layer (the air facing layer) is fluoro-containing polymers for strong weatherability performance. Fig. 14 presents a typical cross section of a commercial backsheet structure.

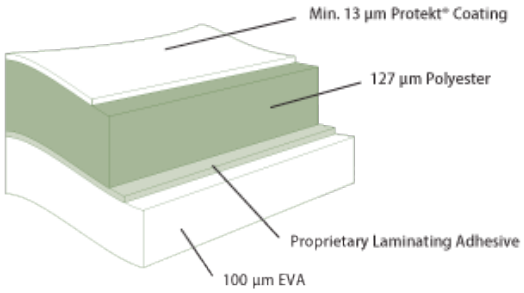

Fig. 14. A typical backsheet structure.[34]

The aging behavior of PV backsheets has not been fully understood to date. The role of UV irradiation, which is a major driving factor of PV module aging, still needs further investigation. In this research, the aging behavior of PV backsheets under UV irradiation will be mainly studied to augment the knowledge base in this area.

1.3. UV Degradation of Low-Density Polyethylene (LDPE)

Research on UV degradation mechanisms of solar panel backsheets is scarce in the literature. Most of the research is focused on either other polymer components of PV modules or degradation under conditions other than UV irradiation (e.g. thermal degradation). Only one paper has been found to be on the exact topic.[35] The backsheet materials that were investigated in this paper include PET, polyvinyl fluoride (PVF) and polyvinylidene fluoride (PVDF). Infrared spectroscopy, differential scanning calorimetry (DSC), and tensile tests were carried out to characterize chemical, thermal and mechanical properties of the backsheets before and after UV irradiation.

Since the backsheet materials that we studied in this project contains mainly low-density polyethylene (LDPE) and ethylene vinyl acetate (EVA), research on the degradation of these

two materials is briefly discussed here. Polyethylene (PE) is widely used as a backsheet for its good dielectric properties, thermal stability, and low cost. As mentioned before, the backsheet in a PV system is exposed to a series of aggressive ambient factors, including UV irradiation, thermal changes, and humidity. As a result, oxidation, crosslinking and degradation occur, and external cracking and internal stresses develop. This behavior, in turn, allows deeper penetration of oxygen and other aggressive ambient factors into the sample and therefore promote aging.[36]

Calorimetric, spectroscopic, and microscopic methods are frequently used, and usually combined with each other to study the aging processes of materials. Oxidation is one of the most important mechanisms in the aging processes. FTIR has been used to characterize and quantify the oxidation products in LDPE,[37] high density PE (HDPE),[38] linear low density PE (LLDPE),[39] metallocene,[39] crosslinked polyethylene,[37,40,41] ultra-high molecular weight polyethylene (UHMWPE),[42] and PE containing various additives[43].

A significant number of papers related to the degradation behavior of PE have been published. The mechanical and kinetic aspects of the PE aging behavior have been exhaustedly discussed by Gugumus[44–50] in a series of papers. PE aging in molten and solid states was both studied. The decomposition of the hydroperoxide group formed in PE processing, which creates free radicals and leads to most of the degradation products, has been rigorously studied in these papers.

The effects of weathering under simulated sunlight on the molecular structures of LDPE and crosslinked polyethylene (XLPE) were identified and quantified with the ATR-FTIR technique by Gulmine *et al.*[41] Lorentzian fitting and Lambert-Beer law were used to develop a reliable methodology to detect and quantify the degradation products of PE. The products,

including cumyl alcohol and acetophenone, and new groups, including carbonyl, vinyl and hydroxyl in the polymer chain, were detected during the degradation of XLPE. The major chemical modification to the tested materials was the formation of different carbonyls, such as ketones, esters, and *γ*-lactones.

The mechanisms of the formation of carbonyl groups have been investigated in the work of Khabbaz[51] (*γ*-lactone), Gugumus[52] (ester), and Lacoste[53] (ketone). *γ*-lactones were formed from reactions between carboxylic acid and hydroxyl group in the 1,4 position or the decomposition of 1,4-dihydroperoxide.[51] The formation of esters was mainly attributed to the condensation reaction between carboxylic acids and alcohols from oxidized LDPE (other polymers can also take this pathway). No mineral acids were necessary as catalysts in this process, and the only requirement was that sufficient amount of carboxylic acids and alcohols were formed from the oxidation process.[52] Vinyl and ketones were both yielded from a chain scission through Norrish II mechanism[44,53], as shown in Fig. 15.

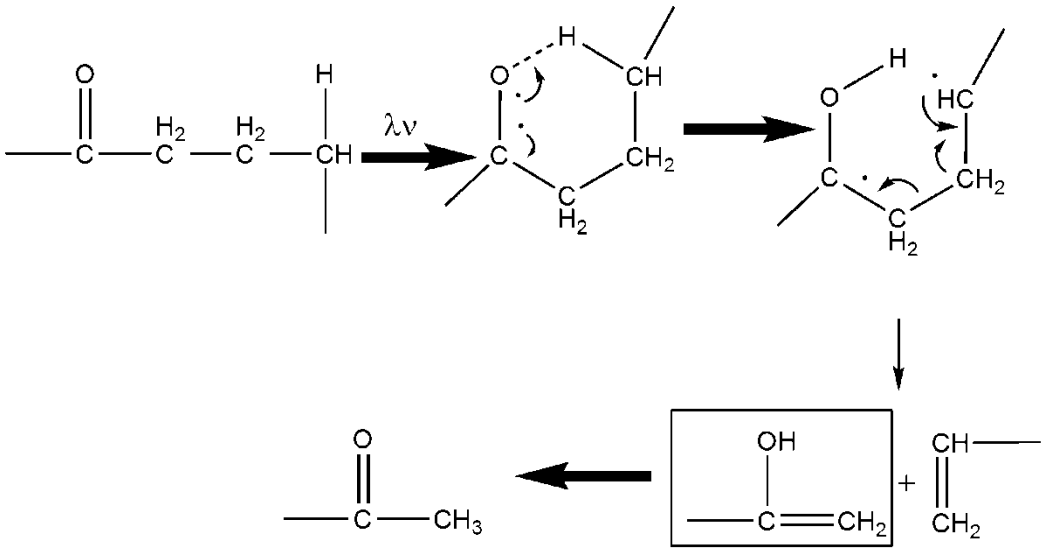

Fig. 15. Illustration of Norrish II mechanism

UV-degradation is a combination of photolysis and oxidative reactions.[54] Which one dominates the process depends on the composition of the atmosphere and the types of polymers. In the presence of air, most polymers undergo photooxidative degradation, which is faster than pure photolysis degradation. Photooxidative degradation is a radical-based autooxidative process (see Fig. 16), which can be divided into four stages: initiation, which includes direct initiation and initiation from oxidative impurities; chain branching and propagation, which are both repeating process whose position depends on the most labile carbon-hydrogen bond on the polymer; and termination, which is the reaction between two peroxy radicals and in which several different byproduct can be created, including dialkylperoxides (from tertiary peroxy radicals, as in polypropylene), alcohol and ketone (from secondary peroxy radicals, as in PE and polyamide 6).[54]

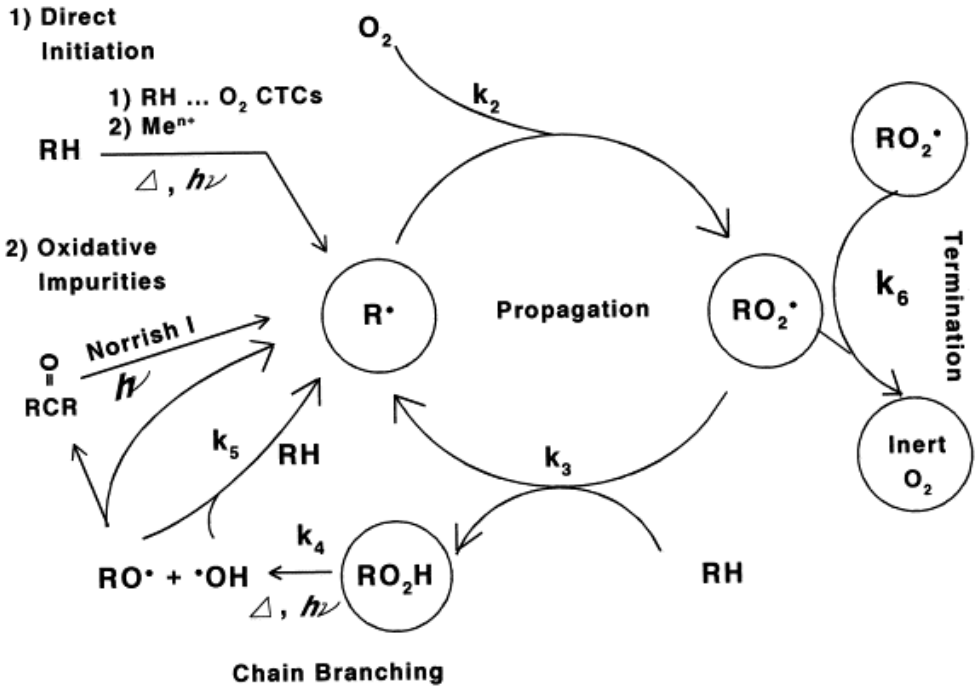

Fig. 16. Autoxidation mechanism for almost all polymers (R = polymer chain, H = labile hydrogen, X• = any radical, ki = reaction rate).[54]

1.4. Degradation of Ethylene Vinyl Acetate (EVA)

In the 1980s, researchers from Flat-Plate Solar Array Project (FSA) in the Jet Propulsion Laboratory (JPL) tested a series of candidate encapsulation materials and developed EVA as an inexpensive alternative to PVB and silicone encapsulants, which undergo delamination during outdoor exposure.[55–58] Since then, EVA has been used as the dominant encapsulation material in PV cells for electrical isolation, mechanical support, optical coupling, and protection against environmental exposure.

EVA was chosen mainly because of its low cost.[59] However, since the late 1980s, the discoloration of EVA encapsulants of outdoor PV modules has been observed.[60–62] In addition to that, researchers also found that there are several other problems limiting the performance of EVA as an encapsulant. For example, under ultraviolet irradiation or atmosphere water, EVA tends to decompose to produce acetic acid at a very low rate, lowering the pH and causing corrosion and module deterioration. Another problem is that under temperatures lower than 15 °C, EVA undergoes glass transition and its modulus increases, which makes a PV module more vulnerable to physical stresses such as those applied by wind or snow. Other drawbacks of EVA include non-ideal thermal and mechanical properties, the need for vacuum lamination in production, and a high diffusivity of water.[63]

Thermal degradation mechanism of EVA copolymer nanocomposites has been studied. In the initial stage of degradation at ~350 ^{o}C, EVA gives off acetic acid, yielding poly(ethylene-co-acetylene) with C=C bonds along the backbone chain. At around 450 ^{o}C, EVA undergoes allylic scission reaction. The result from these reactions is the formation of allylic radicals and

diradicals, which can be rearranged into secondary allylic radicals, whose structure is more stable (Fig. 17).[64]

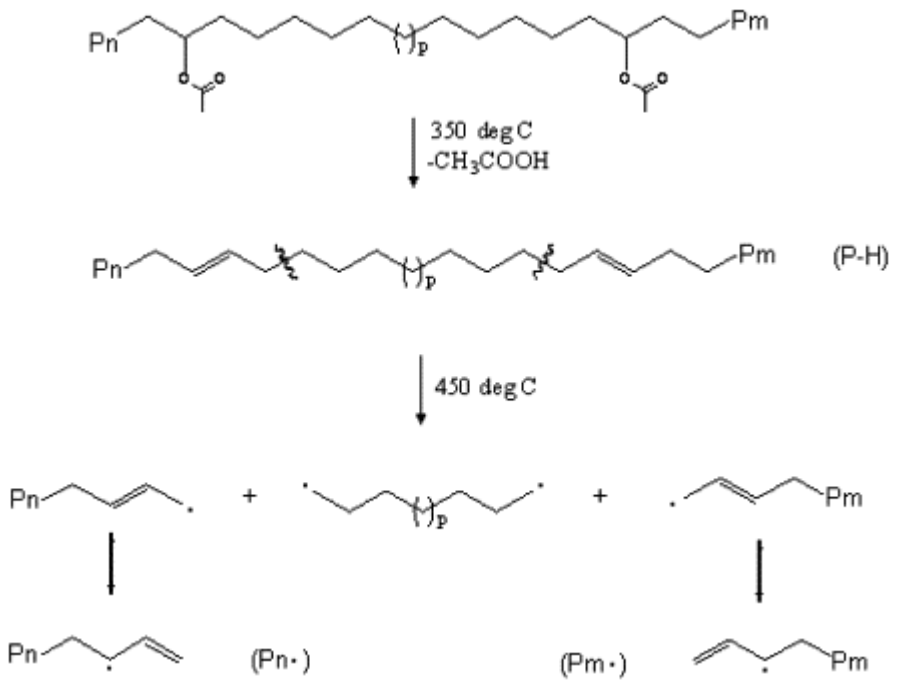

Fig. 17. Illustration of thermal aging mechanism of EVA by allylic scission of the backbone chain.[64]

The diradicals can undergo either hydrogen abstraction by radical transfer with the original reactants, or hydrogen loss by disproportionation, yielding n-alkanes, α,ω-dienes and terminal olefins (Fig. 18).[64]

The secondary allylic radicals can undergo radical transfer reactions with the initial reactants, where the new radicals can revert to the aging cycle, and undergo additional scission, etc.[64]

Photodegradation of EVA undergoes a similar process. The mechanism is shown below in Fig. 19 and Fig. 20. The major reactions include Norrish I, yielding acetaldehyde, CO, CO_2, and CH_4, and Norrish II, producing acetic acid and polyenes.[65]

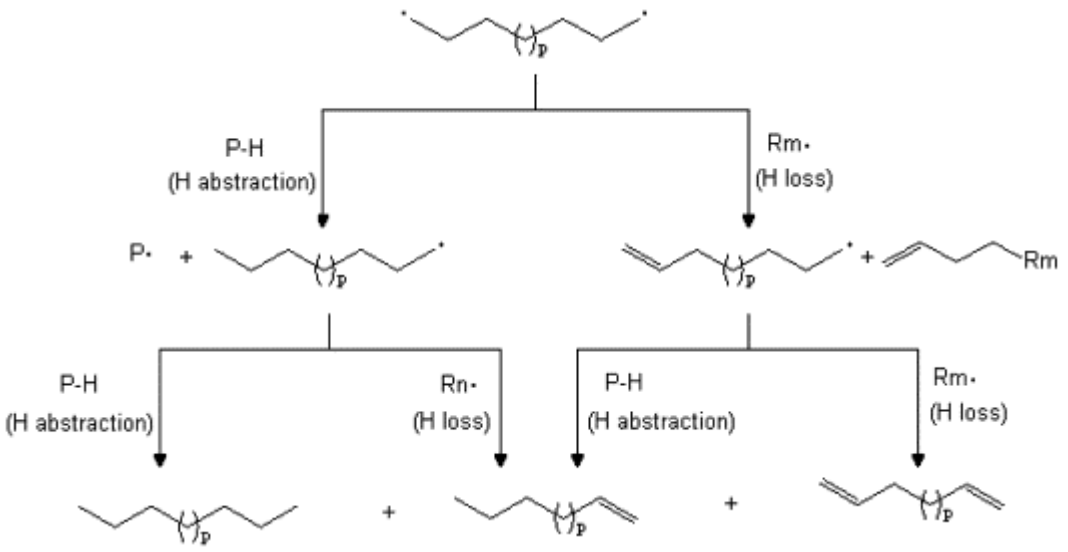

Fig. 18. Illustration of further degradation of EVA: diradicals.[64]

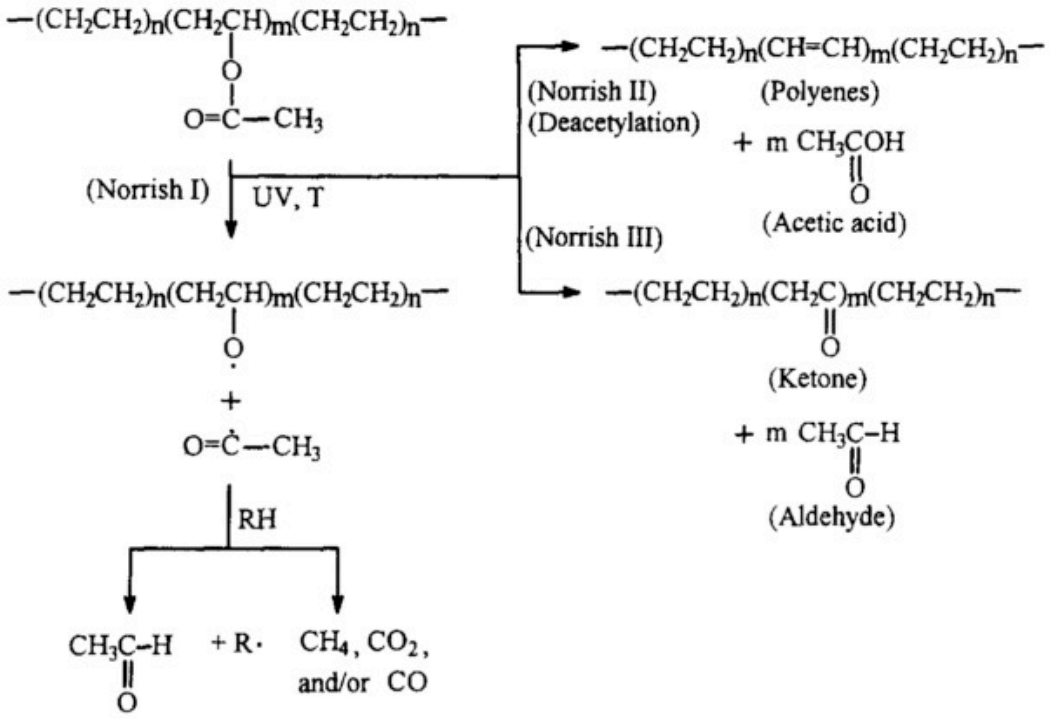

Fig. 19. Illustration of aging mechanisms of EVA, yielding carbonyl compounds and gases.[65]

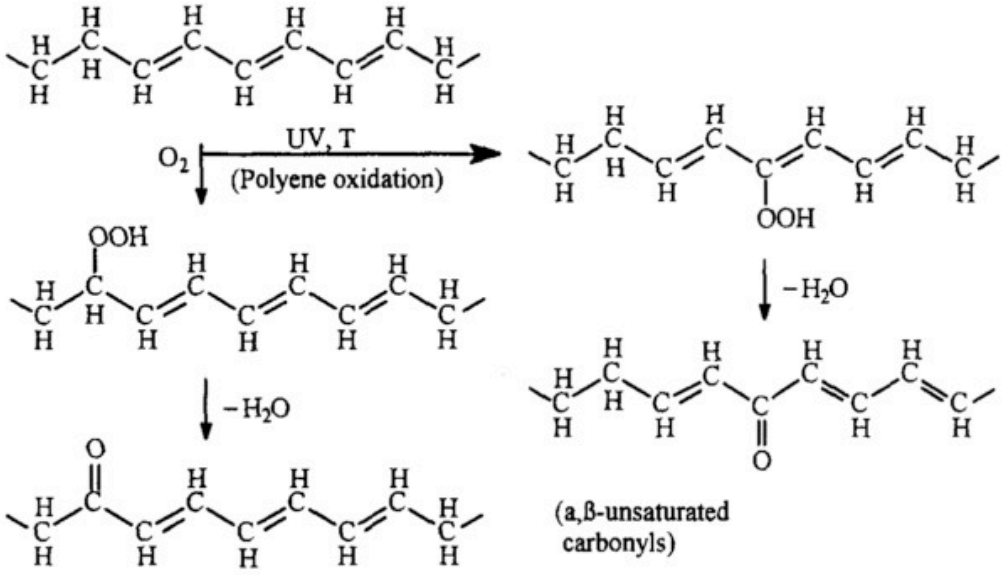

Fig. 20. Illustration of aging mechanisms of EVA, yielding unsaturated carbonyls.[65]

1.5. Fourier Transform Infrared Spectroscopy (FTIR) Theory and Applications

Fourier transform infrared spectroscopy (FTIR) is a special type of infrared spectroscopy, which is commonly used to identify chemicals based on their characteristic absorptions of IR spectrum. These absorptions occur at resonant frequencies, i.e. the frequencies of the absorbed irradiation match the transition energy of the vibrating bonds or groups. The absorbed energies are determined by the masses of the atoms, the bond types, and the modes of motion. A bond can have multiple motion modes. For example, in a CH_2X_2 group of an organic material (where X represents an element other than C and H), there are nine different vibration modes in total for the whole group, with six of them involving only CH_2 and the other three involving the C-X bond. These vibration modes include symmetric and asymmetric stretching, scissoring, rocking, wagging, and twisting.

Infrared spectrometry has evolved remarkably over the past 50 years.[66] In 1957, the Perkin-Elmer Infracord was produced as the first low-cost spectrophotometer which can record an infrared spectrum.[67] FTIR is a technique to obtain an infrared spectrum of absorption, photoconductivity, emission, or Raman scattering of materials in any state (solid, liquid, or gas). It is developed based on the basic infrared spectrometry technique and has become a major approach to get chemical bond information from samples. Instead of shining a beam of monochromatic light at the sample at a time, recording the absorption of that beam by the sample, and repeating the process at a spread of wavelengths, like the dispersive (scanning) spectrometer, FTIR shines a beam consisting of a range of frequencies of light at once, and measures the absorption. Then, another beam containing a different combination of frequencies is shone, and a different absorption is recorded. After repeating the process several times, a computer converts the data into the spectrum using Fourier transform and gives the absorption at each wavelength.

CHAPTER 2. RESEARCH OBJECTIVES

As briefly discussed in Chapter 1, the current flat PV module certification test standards of IEC61215, IEC61730-1 and 2, and UL1703, do not adequately address the UV/light stability of the PV module as well as the module subcomponents, especially the polymeric subcomponents such as encapsulant and backsheets. The objective of this study is to work with Task Force 5 in the International PV Module Quality Assurance (QA) to develop a method to perform accelerated UV aging tests for the evaluation of long term durability of polymeric backsheets. Chemical, electric, optical and morphological properties of the backsheets under different aging conditions will be studied. A practical modeling method to analyze the overall aging behavior and to predict the UV stability of the backsheets will be established.

CHAPTER 3. MATERIALS AND METHODS

3.1. Materials

The solar panel backsheets studied in this research are all commercial products. All backsheets are typical three-layer laminates. The inner layers (sun facing layer) are made of either EVA or LDPE and the bottom layers are made of a fluoropolymer for improved weatherability. Four backsheets, labelled as C, K, M2 and T (Fig. 21), were studied in this project. Supplier origins of each sample are shown in Table 2. The detailed compositions of the backsheet materials are not available because of the confidentaillity of material information.

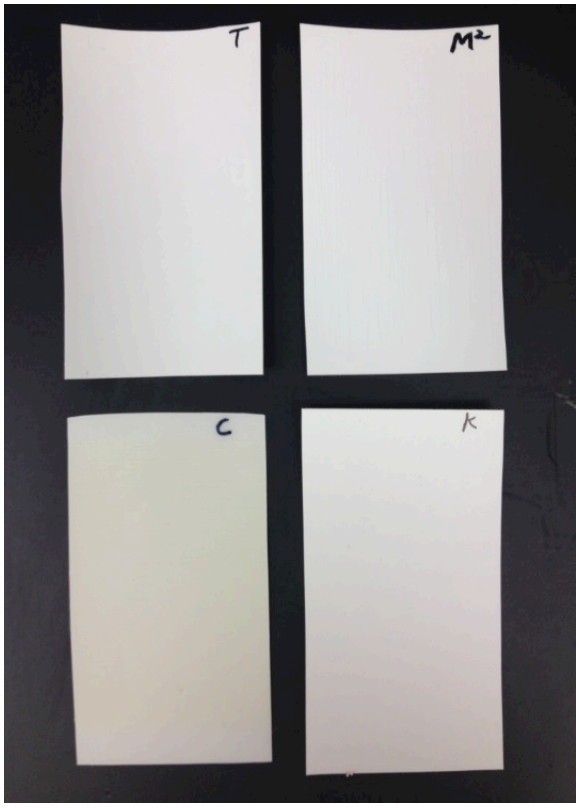

Fig. 21. Photos of the four backsheet samples after 1000 h UV irradiation.

Table 2. Supplier origins of the four backsheet samples.

Sample Code	Suppliers
C	US supplier
K	Japanese supplier
M2	US supplier
T	Japanese supplier

3.2. Ultraviolet Irradiation Aging Test

The four samples were cut into rectangular pieces of 45 mm × 80 mm and loaded into a QUV-SE Accelerated Weathering Tester (Q-Lab) (Fig. 22), where the inner layer was exposed to the UV light source continuously. The QUV tester was chosen because it is easy and affordable to operate, and the fluorescent UVA-340 lamps of the tester give the best simulation of the effects of sunlight in the critical short wavelength region from 365 nm to

295 nm. Aging tests were performed at a UV light intensity of 0.35 W/m^2 at 340 nm for 0 h, 500 h, 1000 h, 1500 h, 2000 h, 2500 h, and 3000 h. The 0.35 W/m^2 intensity was chosen because it is the most commonly used UV intensity for polymer/plastic material aging per UL746C and other standards.[68,69] The temperature was held constant at 60 °C, following IEC 61215 UV-precondition requirement[20].

Fig. 22. QUV-SE Accelerated Weathering Tester (Q-Lab).[70]

3.3. Optical Microscopy

In order to study the morphology of the aged and pristine sample surfaces, optical microscope observation was carried out using an Axiovert 40 MAT microscope equipped with a ProgRes C10 plus digital camera. Micrographs of the surfaces were analyzed using iSolution DT image analysis software.

3.4. Shrinkage Rate Testing

Shrinkage rate testing was carried out on the original backsheets to characterize the amount of residue stress in the materials. A sample pan with a layer of sand on its bottom was put in a Squaroid vacuum oven and the oven was preheated to 150 °C. The backsheets were cut into 10 cm × 10 cm samples with an accuracy of 0.1 mm. Three measurements on each direction were made to obtain average dimensions. The samples were then laid on the sand in the sample pan, heated for 3 min at 150 °C, removed from the oven and let cool naturally for 2 h. The samples warped to a small degree after the heat treatment but were pressed flat when the dimensional measurements were conducted at the same positions taken before. The shrinkage rates in the machine direction and transverse direction were calculated using $(D_b - D_a) / D_b$ (D_b: size before heat; D_a: size after heat) based on the average dimensions.

3.5. Scanning Electron Microscope (SEM)

A JEOL JSM-6490LV scanning electron microscope was used to study the microcracks on the sample surfaces created by UV irradiation. The four sets of virgin backsheets and the ones after 3000 hours UV irradiation were observed and compared. This serves as a qualitative way of characterizing the physical integrity of the backsheets

3.6. Color Change (Yellowness Index and Delta E) Analysis

Color changes of the aged samples were measured using a Macbeth Color-Eye 7000 Spectrophotometer with an aperture diameter of 2.54 cm. A flash was projected on sample surfaces and the reflected light was collected and analyzed. Calibrations using a zero

calibration standard (light trap) and a total reflection standard (white board) were performed before every measurement. Every measurement of a single sample was repeated three times by measuring at different locations of the sample. The reported YI was the average values calculated from the three measurements using Equation (1). The coefficients C_x and C_z in Equation (1) were to be 1.2985 and 1.1335, respectively, based on the standard illuminator and observer used in this instrument (D_{65}, 1931).[32]

3.7. UV-Vis-NIR Spectrum Analysis

Macbeth Color-Eye can only measure visual color changes, i.e., the changes of the reflection ranging from 390 nm to 700 nm. In this study, a Cary 5000 UV-Vis-NIR spectrophotometer was also used to observe sample color changes within a wider spectrum. The reflectance accessory (DRA-2500 from Varian) used in the spectrophotometer exhibited a sample port size of 16 mm in diameter. The range of the spectrum spreads from 250 nm to 1200 nm, which is the major functional range[71] of PV cells. The scan was taken in reflection mode with 0.1 s of scan time per point on average. The reflection is also another important factor when evaluating backsheet materials. Usually, for better energy harvesting, one will desire that the backsheets exhibit high level of reflection thus the light reaching the backsheets can be re-directed back to the active cell area to generate electricity. The contribution to the power output from the reflection of the backsheets can reach around 2%.[31]

3.8. Fourier Transform Infrared Spectroscopy (FTIR)

FTIR analysis was performed on a Nicolet 6700 FTIR Spectrometer (Thermo Scientific, Waltham, MA) operating on a resolution of 4 cm^{-1} and 32 repetitive scans. The FTIR spectrometer was equipped with a deuterated triglycine sulfate (DTGS) detector and the spectra were obtained using a Smart Performer ATR accessory equipped with a 45º ZnSe crystal. Spectrum analysis was carried out with the assistance of OMNIC 7.0 (Thermo Scientific, Waltham, MA). The analysis is used to examine the changes in chemical bondings of the inner EVA or LDPE layer due to the UV aging effect.

3.9. Dielectrical Test

Electrical properties are important performance factors in evaluating backsheets. In addition to mechanical protection, another major function of backsheet is to provide electrical insulation. To study the effects of UV aging on the electrical properties of the backsheets, dielectrical tests were carried out using an Alpha-N High Resolution Dielectric Analyzer (Novocontrol Technologies). The samples were cut into disks with a diameter of 20 mm, and then sandwiched between two copper electrodes with the same size of the sample. Electrical properties such as conductivity, capacity, and resistance were collected under ambient conditions and processed using WinDETA software (Novocontrol Technologies).

CHAPTER 4. RESULTS AND DISCUSSION

The effects of UV irradiation on the optical, chemical, physical and electrical properties of the four commercial backsheets were characterized and are presented in this chapter.

4.1. Visual Inspection and Optical Microscopy

Fig. 23 shows a photo of all four samples after 0, 1500, and 3000 hour UV irradiation. It is obvious that Sample C underwent significant yellowing and a closer look reveals a large number of parallel cracks on the sample surface. Sample M2 shows slight yellowing after 3000-hour irradiation and a considerable amount of parallel cracks can also be noticed. On the other hand, Samples K and T show no sign of color change to the naked eye. Fine cracks are still discernable on Sample T, but only after 3000-hour UV irradiation, whereas no cracks show up at all on Sample K. The visual observation results imply that Sample K is the most UV-resistant backsheet material, followed by Sample T and M2. Sample C shows the lowest UV resistance.

Optical micrographs of the four backsheets after different length of UV irradiation are compared in Fig. 24. First of all, micro-sized particles can be clearly seen on Samples C and M2. These particles are inorganic pigments added into the backsheet materials to give them white color. Similar particles do not appear on the photos of Samples K and T possibly because much smaller particle sizes (e.g. nanosized pigments) are used in these two samples.

	Virgin sample	After 1500 hour	After 3000
C			
K			
M2			
T			

Fig. 23. Photo of virgin Sample C, K, M2, and T and the four samples after 1500 h UV irradiation and 3000 h UV irradiation. 3000 h Samples are partially enlarged in the rectangles with black borders for a better view of the cracks.

Surface cracks develop on all the samples except Sample K. For Sample C, cracks can be seen as early as 500 h, which is the earliest among all the samples. The width of the cracks increases with irradiation time (1000 h) and more fine cracks develop with increasing time. Sample M2 shows a similar crack developing trend with the number and width of the cracks increasing with the irradiation time. Many of the cracks are parallel to each other and show similar width, which is a typical failure mode due to the orientation of polymer chains formed during film extrusion process. These microscopic results agree with those from direct visual observation. The cracks on Sample T appear to develop at a lower rate compared to Samples C and M2. They occur after longer irradiation (1000 h) and their density and width appear to be smaller. For Sample K, no surface crakes can be observed at all during the entire irradiation process. The cracks on the three samples are caused by irradiation induced polymer degradation and the resultant decreases in mechanical properties. The cracks propagate under the influence of the residue stress resulted from the orientation/stretching effect of the film extrusion.

Shrinkage rate testing is a simple method to characterize how much residue stress is present in the samples. For the backsheet application, one would prefer a low shrinkage. In Table 3, Sample K shows relatively uniform shrinkage on both machine and transverse directions, indicating similar chain orientation and strength in both directions. For the other samples, the shrinkage rate in one direction is obviously higher than that in the other direction, implying a preferential crack growth. Usually the higher the stretching/orientation in one direction, the weaker the inter-molecular strength in the transverse direction, thus it is quite normal to observe crack lines parallel to the machine direction for the stretched samples.

Time/ h	C	K	M2	T
0	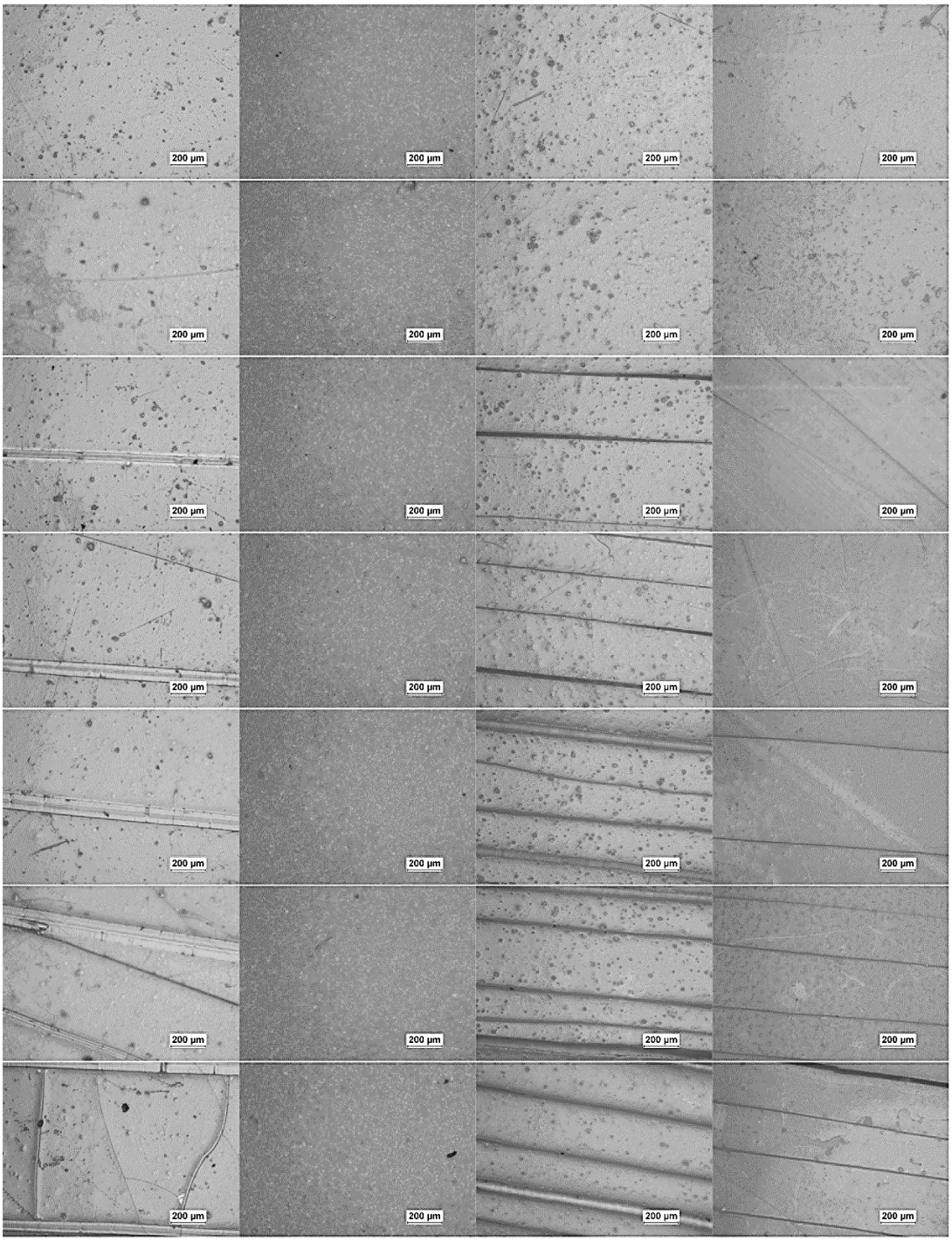			
500				
1000				
1500				
2000				
2500				
3000				

Fig. 24. Optical microscopic photos of the four samples under different dosages of UV irradiation.

Table 3. Shrinkage rate (%) of the samples.

	Machine direction	Transverse direction
C	0.8	0.5
K	0.6	0.6
M2	1	0.5
T	1.2	0.1

4.2. SEM

SEM was carried out to study the microstructures of the cracks caused by UV irradiation. SEM micrographs of the four samples are shown from Fig. 25 to Fig. 28. Fig. 25 shows the microcracks on Sample C after 3000 h irradiation. Being a multilayer laminate, the backsheet shows irradiation induced cracks on both top and the second layers (Fig. 25a). The cracks on Sample C propagate in random directions and intersect with each other. Small cracks can be seen branching out from main cracks (Fig. 25b). The surfaces of Sample C are smooth and clean. The fracture surfaces of the cracks are also relatively clean, showing no sign of extensive plastic deformation (Fig. 25d).

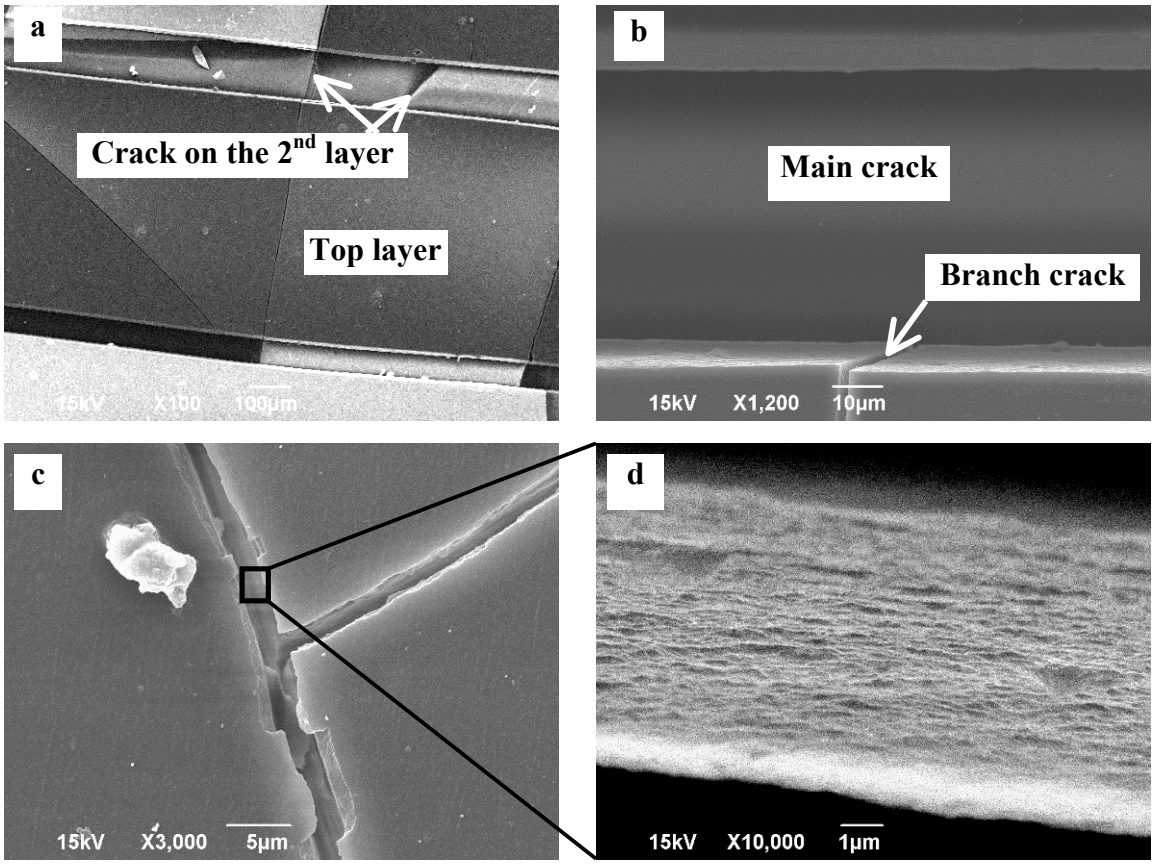

Fig. 25. Sample C after 3000 h UV irradiation.

The surfaces of Sample K are rougher than those of Sample C (Fig. 26). This can be attributed to different materials and processing parameters. Comparing pictures c - d to a - b, no obvious surface microstructure changes can be seen, indicating negligible UV degradation of the sample.

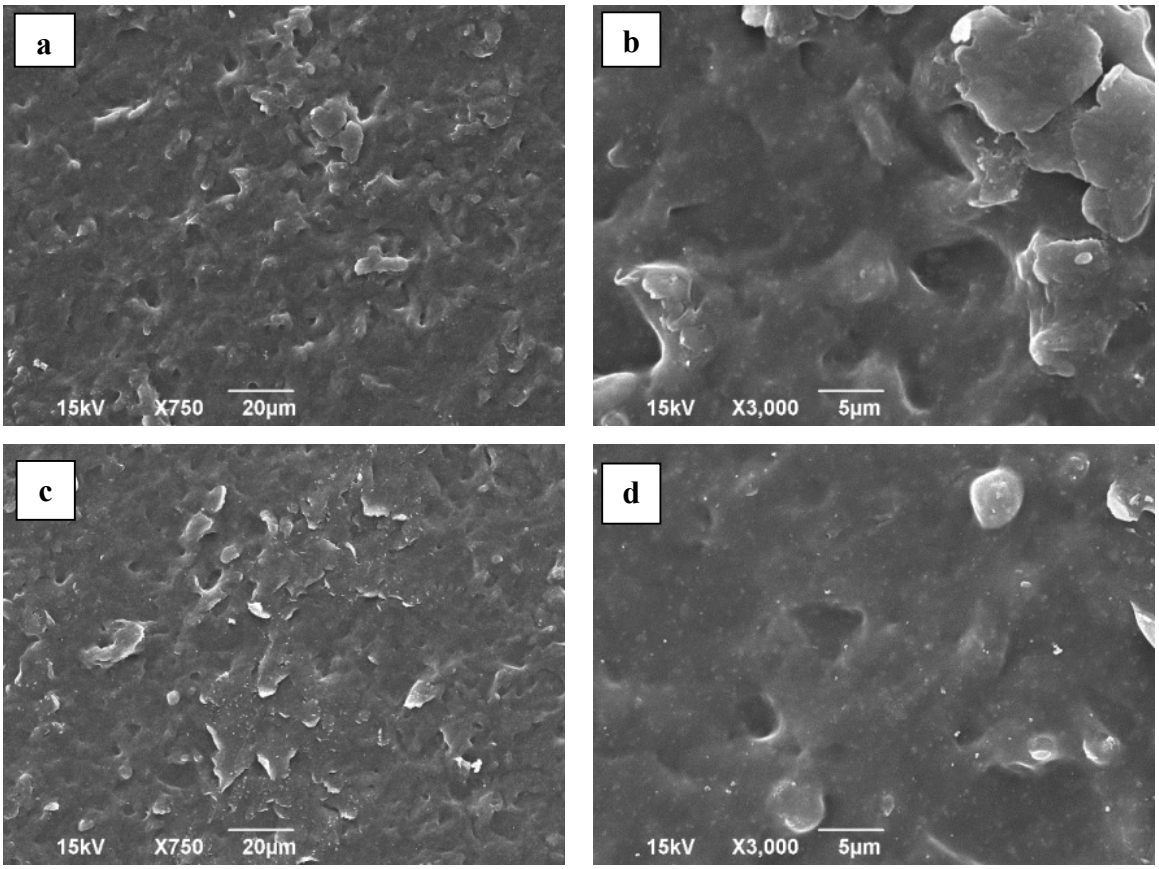

Fig. 26. Sample K in pristine state (a and b) and after 3000 h UV irradiation (c and d).

Similar to Sample C, Sample M2 exhibits many cracks and crack branches on its surfaces (Fig. 27). Crack surfaces are clean and show no sign of plastic deformation. Fig. 27c appears to show delamination of the multilayer sheet after UV irradiation because of the existence of the ligament-like structures (in the circle), which implies the detachment of the top layer from the layer beneath it.

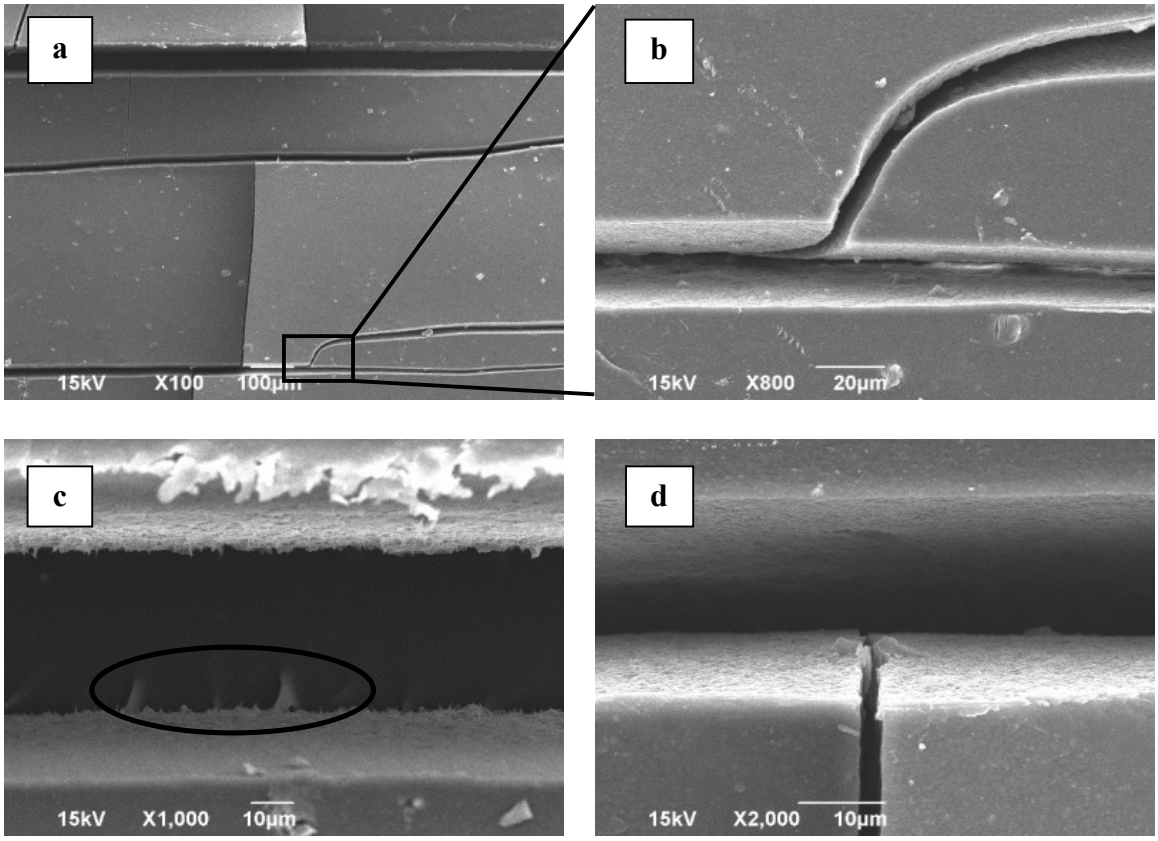

Fig. 27. Sample M2 after 3000 hour irradiation.

Sample T shows smaller number of cracks (Fig. 28) compared to Samples C and M2. Major cracks are connected by propagating small cracks (Fig. 28a and d). The branch crack in Fig. 28b appears to be shallower than its root crack. Large number of ligaments can be seen at the bottom of the cracks (Fig. 28a, b and c), indicating delamination within the multilayer structure.

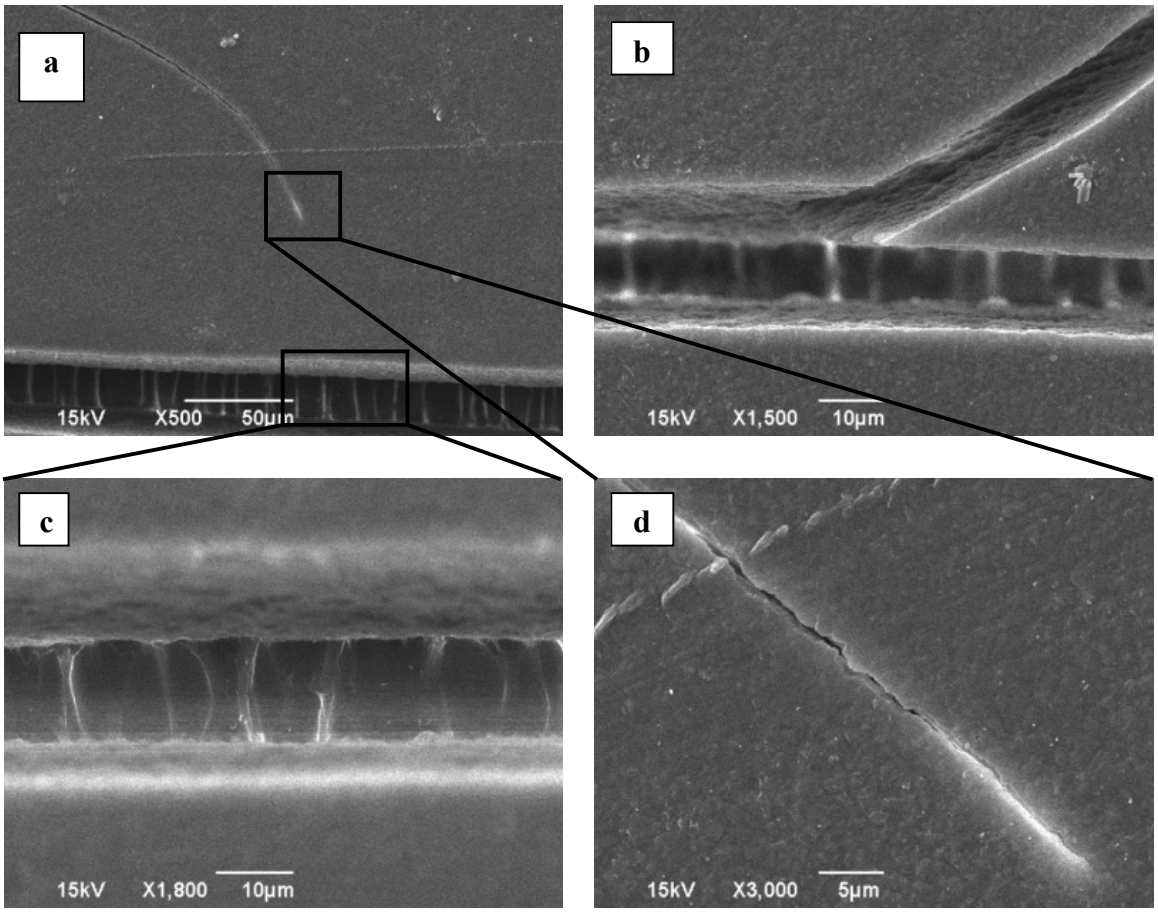

Fig. 28. Sample T after 3000 hour irradiation.

4.3. YI (Yellowness Index)

Before we discuss about the quantitative effect of UV dosage to the YI change of the samples, let's explain how to calculate the UV dosage.

Per spectral power distribution of lamp UVA-340[70], with lamp intensity setting of 0.35 W/m^2 at 340nm, the integrated total UV dose from 280nm to 400nm is about 20 W/m^2. The total UV dosage (TUV) with different UV aging time can be simply expressed as:

$$I = 20\ W/m^2 * \text{aging time (in 1000 hours)}\ (kWh/m^2) \quad (2)$$

where I is the UV irradiation dosage.

The UV dosage and different irradiation time were tabulated in Table 4. As a reference, the annual total UV dosages in Arizona (representative hot and dry region) and Florida (representative hot and humid region) are 93 kWh/m^2 and 78 kWh/m^2, respectively.[72]

Table 4. The UV dosage for different irradiation time.

Irradiation time (hour)	**0**	**500**	**1000**	**1500**	**2000**	**2500**	**3000**
UV dosage (kWh/m^2)	**0**	**10**	**20**	**30**	**40**	**50**	**60**

Fig. 29 shows the YI of the four samples as a function of UV dosage. The figure shows that for all the samples, their YIs increase with the dosage. Sample C exhibits the highest increase rate while the rates of the other three samples are similar and close to zero. In fact, the YI values of the three samples over the entire dosage range are all close to zero, indicating that the yellowing behavior of the three samples is negligible and the UV resistance of the sample is outstanding under the testing conditions. The great difference of the yellowing behavior between sample C and the other three samples showed the importance of engineering evaluation for the materials: all four samples are commercial products with similar laminate structures and are all claimed to be able to function in fields for 25 to 30 years. However, from the YI results sample C will definitely not be able to behave as well as the other three competitors. Some negative YI values are shown in the figure, which can be attributed to initial greenish color of the samples (unnoticeable to human eyes because their YI are smaller than 5). The YI results agree well with the morphological results presented in the previous section, i.e. sample C exhibits the weakest UV resistance.

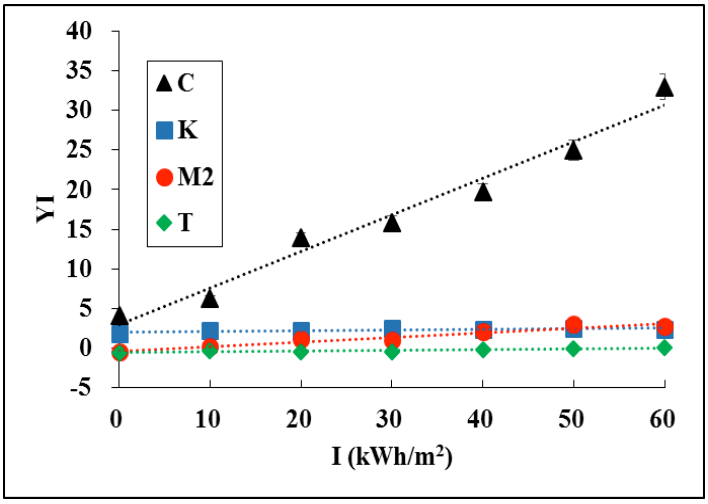

Fig. 29. YI vs. UV dosage of the four samples. Dotted lines are linear fittings of each group of data.

In order to quantitatively estimate the yellowing processes of the backsheets, curve fitting was also attempted for each group of YI data. A linear fitting function was found to be able to properly fit all the data groups:

$$YI=a*I+b \quad (3)$$

Where *a* and *b* are the two fitting coefficients which represent YI increase rate and initial YI values, respectively. *a*, *b* and R^2 (which measures the goodness of the fitting) for each sample are given in Table 5. The linear relationship between YI (which is an indication of degradation degree) and the UV dosage is in agreement with the findings of Daro, who examined the chain scissions per molecule for the polyolefin and found that the number of chain scissions exhibited an linear relationship to the accumulated total solar radiant exposure.[73] Table 5 clearly shows that sample C has the highest degradation rates (at least 8 times higher than the other three samples) and sample K is the most UV resistant sample.

Table 5. Parameters used in linear curve fitting.

	C	K	M2	T
a	0.4630	0.0098	0.0581	0.0104
b	2.9438	2.0216	-0.3102	-0.5476
R^2	0.9739	0.6659	0.9355	0.8233

Currently many UV aging standards for polymers recommend 0.35 W/m^2 for 1000 hours as the aging standard. This is only equivalent to 20 kWh/m^2 total UV dosage, which is about 2.6 months of Arizona UV dosage. This requirement is too low for the outdoor applications of polymeric materials as demonstrated by the increasing YI values in Fig. 29. It is recommended that the hours or the irradiation strength can be increased in the standards so that the samples are tested through higher total dosages.

4.4. Delta E

In addition to YI, Delta E is another commonly used parameter to characterize material color change. While YI can only indicate the color changes between green and yellow, Delta E provides a more comprehensive representation of color change in the visible light range. It can be calculated using the equation below[74]:

$$\text{Delta } E^2 = (L_1-L_2)^2+(a_1-a_2)^2+(b_1-b_2)^2 \quad (4)$$

where L, a, and b are coordinate values in a nonlinearly compressed CIE XYZ color space. L is for lightness and a and b for the color-opponent dimensions.

As shown in the equation, Delta E represents the color difference between Color (L_1, a_1, b_1) and Color (L_2, a_2, b_2). The color difference can be identified by naked eyes when Delta E is over 2.3. In other words, the color difference reaches JND (Just Noticeable Difference).[75]

The Delta Es between the original and UV-aged samples as a function of irradiation dosage are shown in Fig. 30 and Fig. 31. Sample C shows a remarkable color change, in agreement with the results from YI analysis. Delta E of the sample reaches 2.13 (slightly below JND), after 500 h UV irradiation, while Delta Es of all other samples are well below JND, meaning no discernible color changes by naked eyes. The curves show a trend similar to that of YI, i.e. the color changes of the samples increase with increasing irradiation dosage. Sample C exhibits the greatest color change in the four samples, indicating that it underwent the most severe degradation, which has already been shown by the YI results and the microscopic studies. The degree of the color change of Sample C is so much that it dwarfs the other three curves in Fig. 30. For a better comparison between the low Delta E samples, only the curves of K, M2 and T are plotted in Fig. 31. Among the three samples. Sample M2 shows the highest degree of color change, corresponding to the results obtained from the optical microscopic study, where it shows the second highest number of cracks. The differences in the color change between Sample K and T are small. Since Sample K is the most UV-resistant sample and the surface layer of Samples K and T are both made of LDPE (see FTIR section), this result suggests that the color change and surface cracking may not be proportionally related to each other.

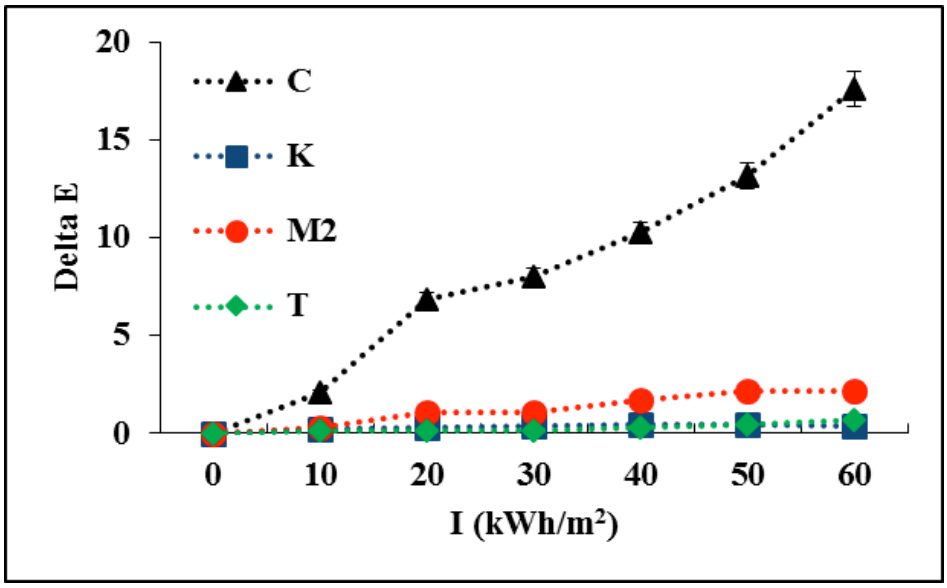

Fig. 30. Delta E as a function of irradiation dosage of all the four samples.

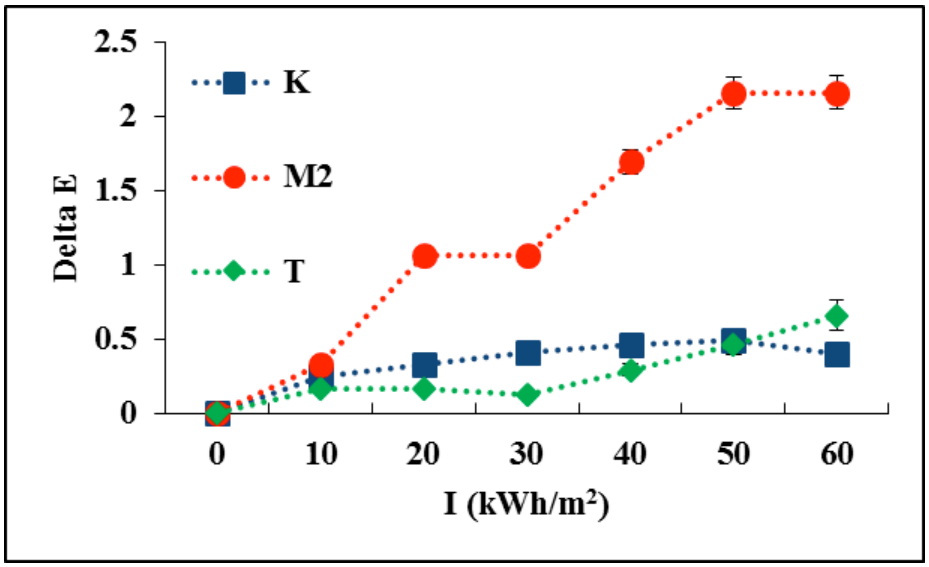

Fig. 31. Delta E as a function of irradiation dosage of Samples K, M2, and T.

Zero corrected YIs (i.e. shifting the lines in Fig. 29 upward or downward so that the initial YI is zero) as a function of Delta E are plotted in Fig. 32 to Fig. 35. It can be easily observed that the two parameters show a linear relationship: YI is about 1.0 to 1.7 times of Delta E. This is true not only for Sample C and M2, but also for Sample K and T, which show

very little color change. This result suggests that these two characterization methods are comparable to each other. This empirical relationship will allow researchers to cross compare samples with only Delta E or only YI. Engineers and researchers have the freedom to choose which is available for them to get the characterization done on the materials under study.

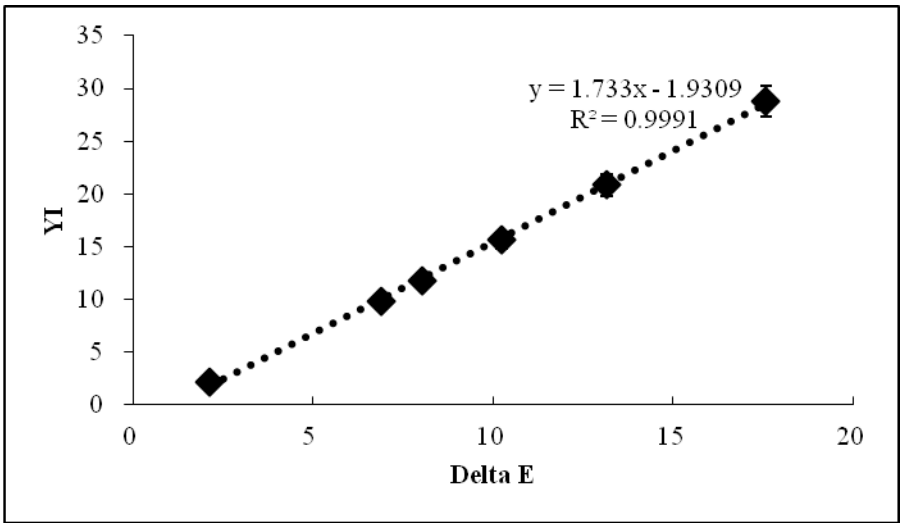

Fig. 32. YI vs. Delta E of Sample C

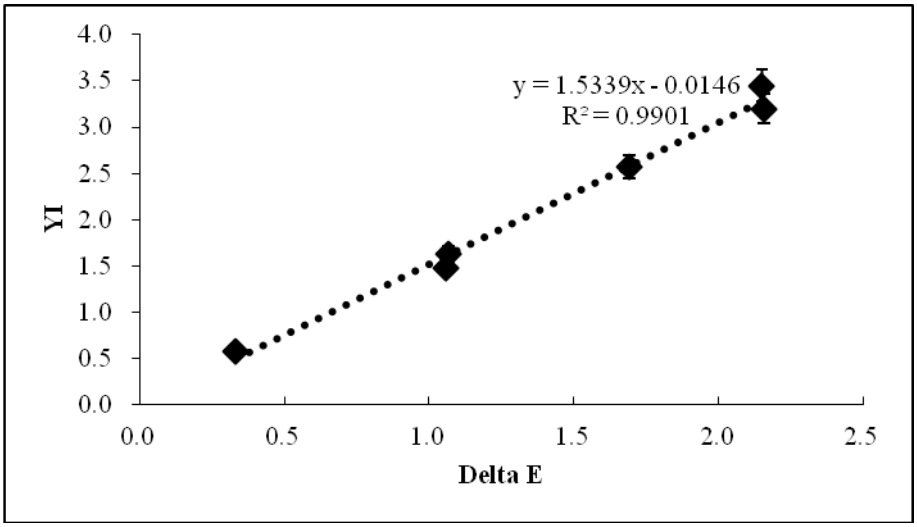

Fig. 33. YI vs. Delta E of Sample M2

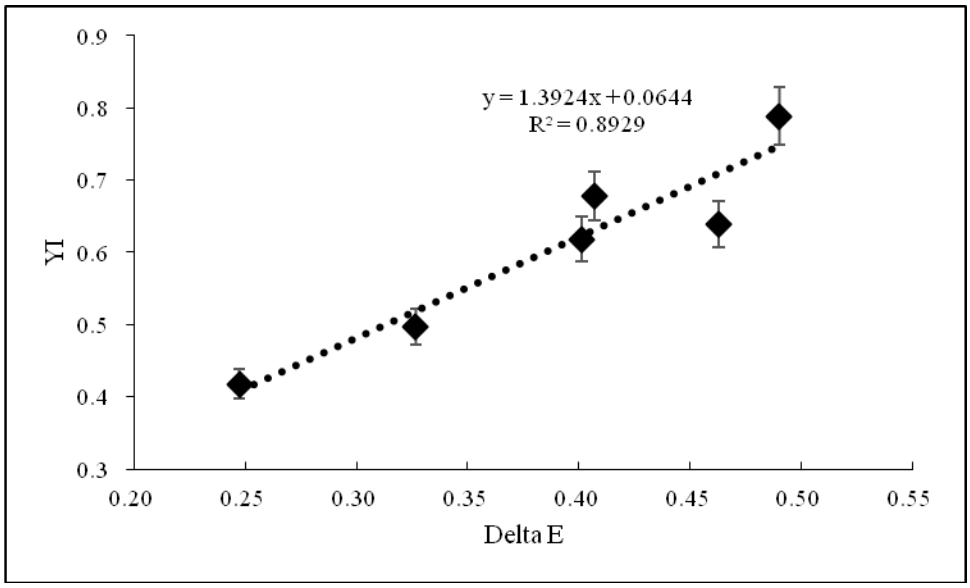

Fig. 34. YI vs. Delta E of Sample K

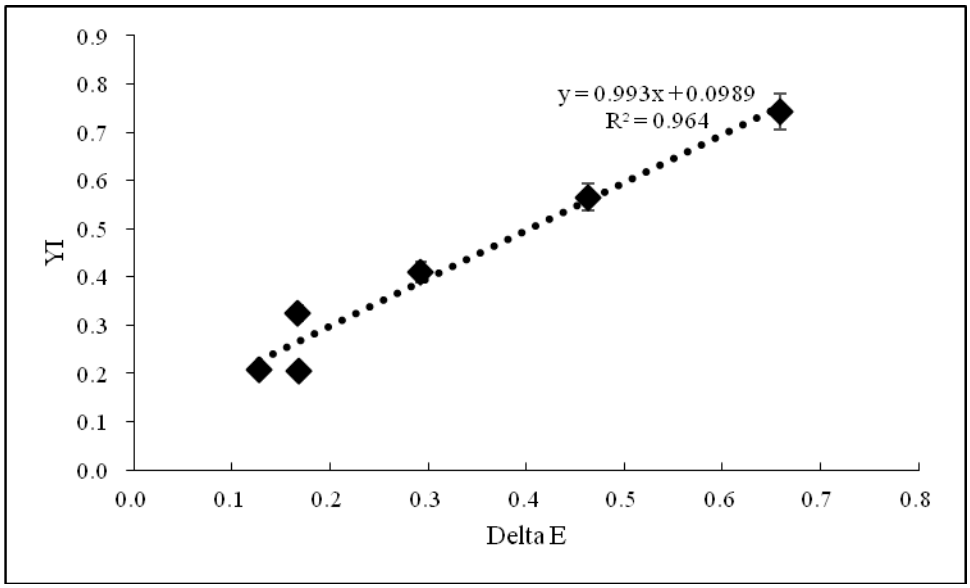

Fig. 35. YI vs. Delta E of Sample T

4.5. UV-Vis-NIR Spectrum Analysis

One function of backsheet is to reflect (re-direct) the light reaching it back to the active PV cell area to generate more electricity. Thus, in general, the higher the reflection of the

backsheet have, the higher the electricity will be harvested, given the same module stack up. The effect of UV aging on the reflection of the backsheet was also characterized here, using UV-Vis-NIR technology. The reflection (R) of Sample C after different hours of irradiation are shown in Fig. 36. The most significant changes (i.e. decease in reflection with increasing irradiation time) occurs within 400 - 600 nm (visible light region). The decreases indicate that increasing amounts of irradiation are absorbed by the backsheets and used to initiate/sustain degradation reactions and to heat up the samples, in both cases promoting material aging. Decreasing reflection also means that PV cells receive less reflected irradiation from the backsheets and therefore generate lower amount of electricity. Sample K, as the most UV resistant sample, shows almost no changes over the entire spectrum (Fig. 37). The reflection decreases for Samples M2 and T (Fig. 38 and Fig. 39) are much smaller compared to C, in agreement with the results obtained before. It is worth noting that only Sample C shows a reflection in the UV (300 – 400 nm) region. This is due to a special UV blocking or absorbing agent used in the sample, which caused this characteristic reflection. The decrease of reflection in this UV range for backsheet C also means that more UV would be absorbed by the aged material, thus accelerating its UV degradation.

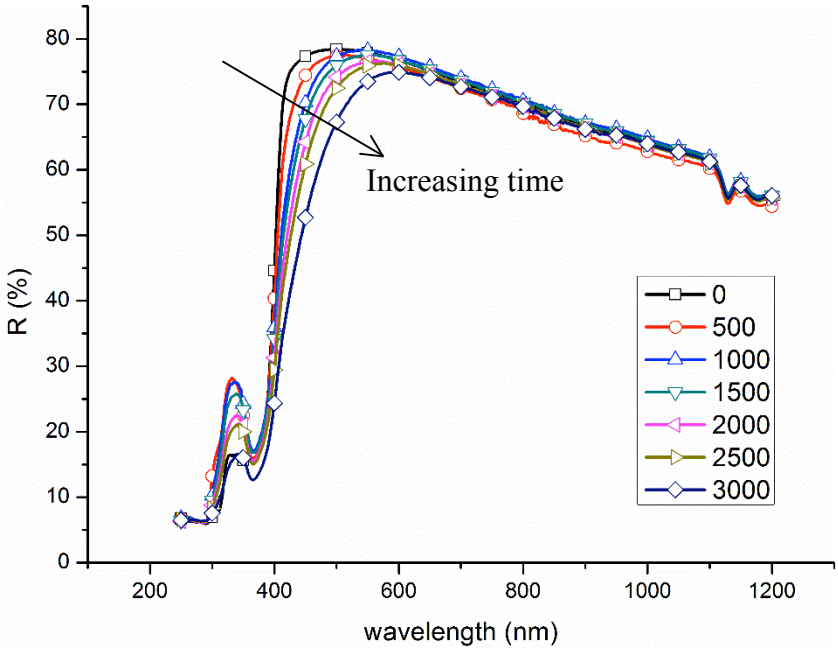

Fig. 36. UV-Vis-NIR Spectra of Sample C.

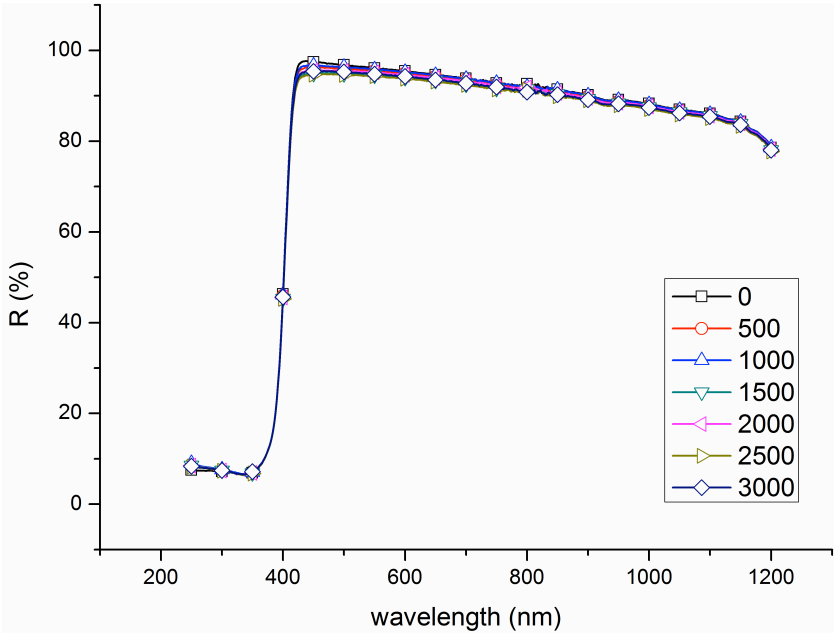

Fig. 37. UV-Vis-NIR Spectra of Sample K.

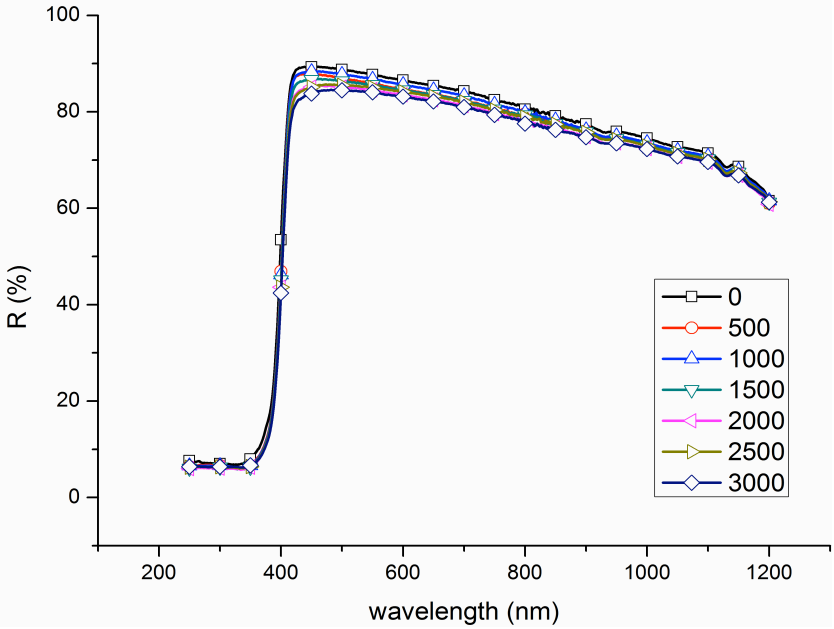

Fig. 38. UV-Vis-NIR Spectra of Sample M2.

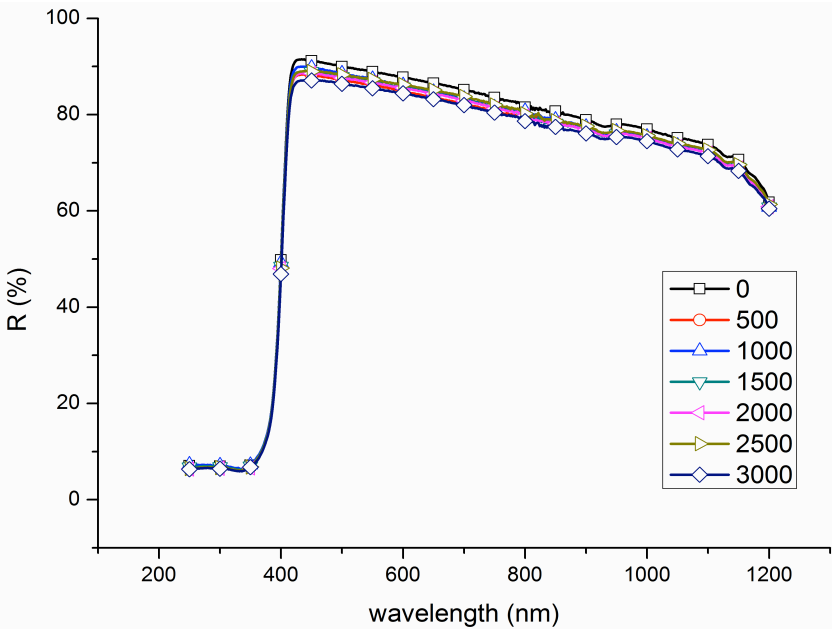

Fig. 39. UV-Vis-NIR Spectra of Sample T.

4.6. Fourier Transform Infrared Spectroscopy (FTIR) Analysis

The color and microstructure changes of the UV aged samples are due to molecular level chemical changes. FTIR is a handy technology for us to check the chemical changes of the four samples. The FTIR spectra of the four samples after baseline corrections are shown from Fig. 40 to Fig. 43. The spectra of Sample C and Sample M2 show the characteristic peaks of EVA, while the spectra of Sample K and Sample T feature the characteristics of LDPE.[76] The peaks of all the samples feature $-CH_2-$ backbone structure: 2915 and 2847 cm^{-1} for $-CH_3$ and $-CH_2$ stretching absorptions, 1472, 1372, and 1461 cm^{-1} for $-CH_3$ and $-CH_2$ bending absorptions, and 729 and 718 cm^{-1} for $-(CH_2)_n-$ rocking absorption with one exception – no 729 cm^{-1} peak on Sample K, which is ascribed to its low n, the degree of polymerization.[76] Those peaks of all four series of samples didn't change much in the process, because the backbone basically remained the same in the degradation.

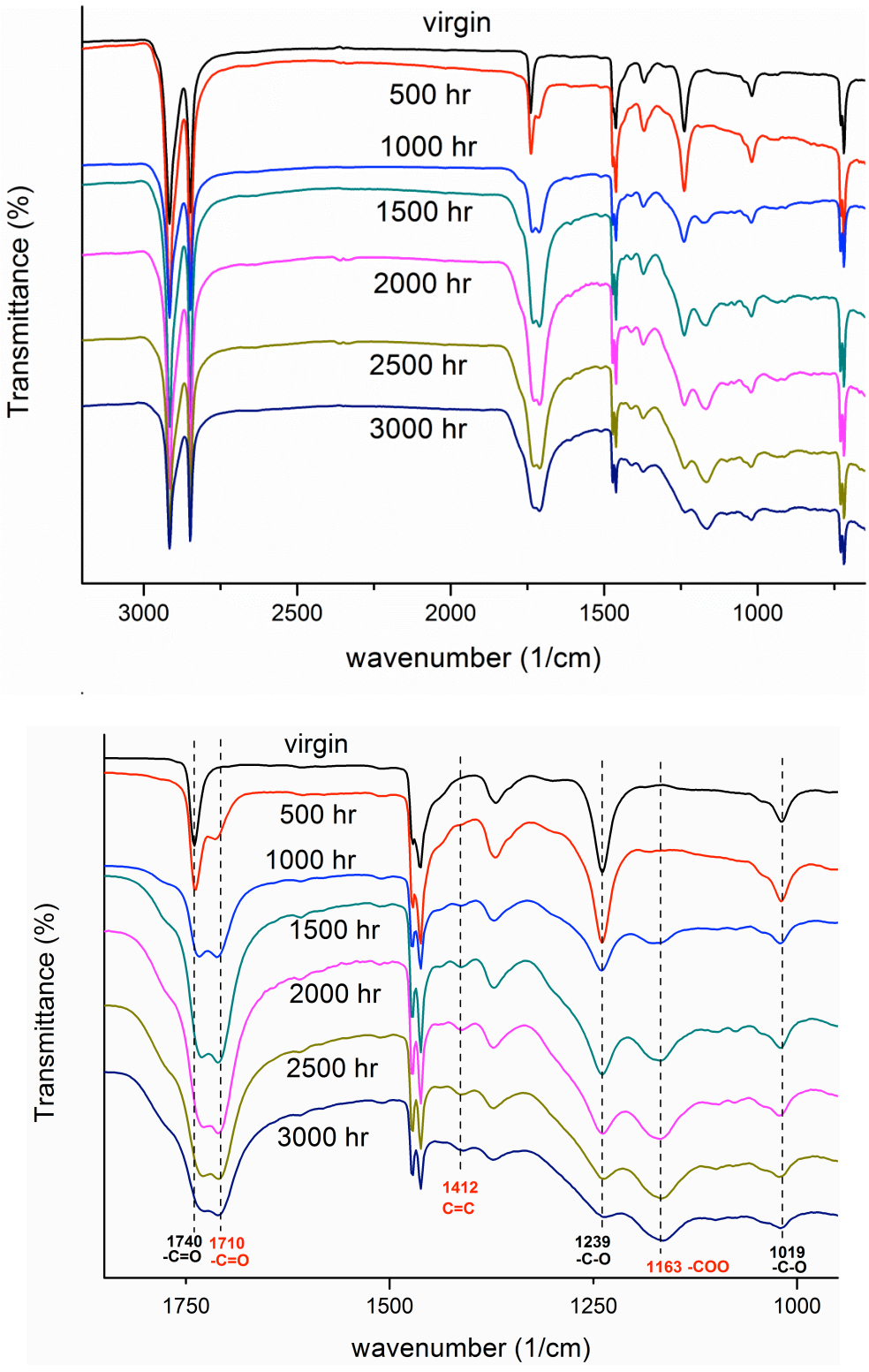

Fig. 40. FTIR spectra of Sample C after different lengths of UV irradiation.

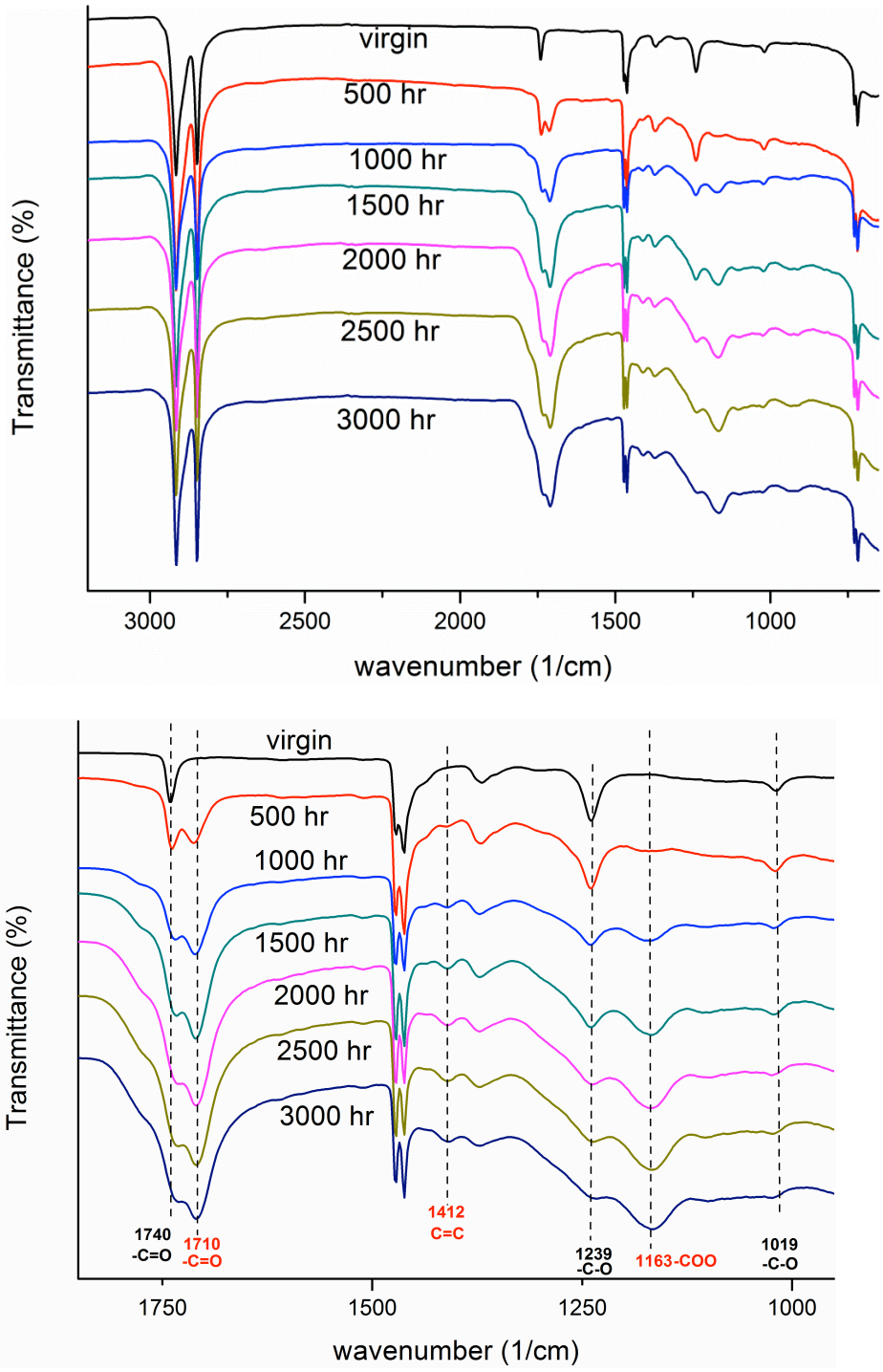

Fig. 41. FTIR spectra of Sample M2 after different lengths of UV irradiation

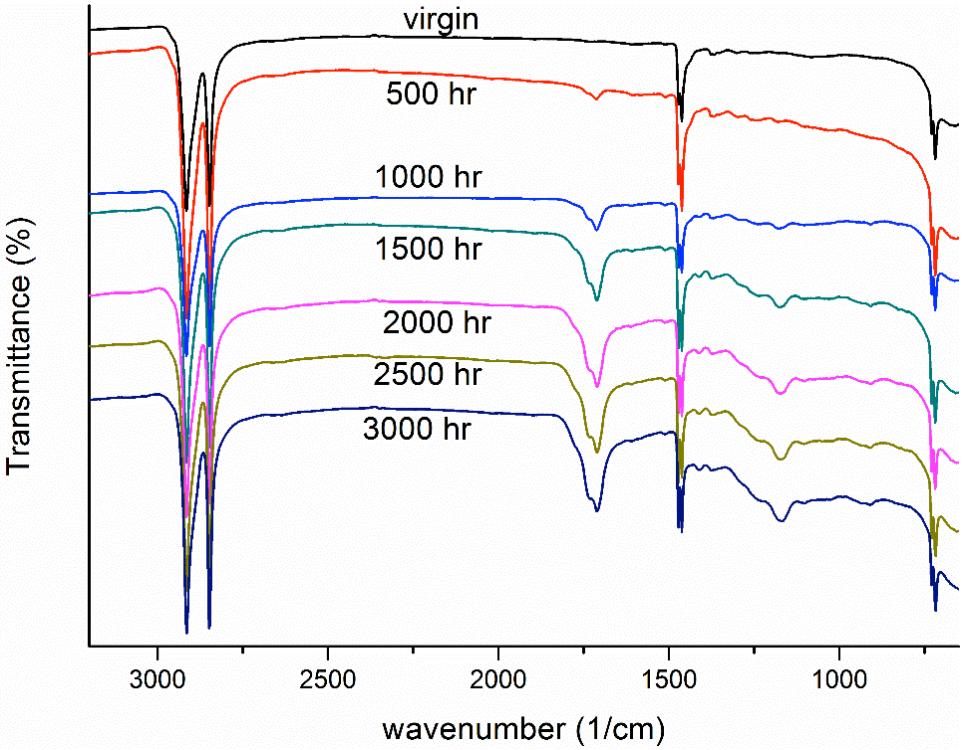

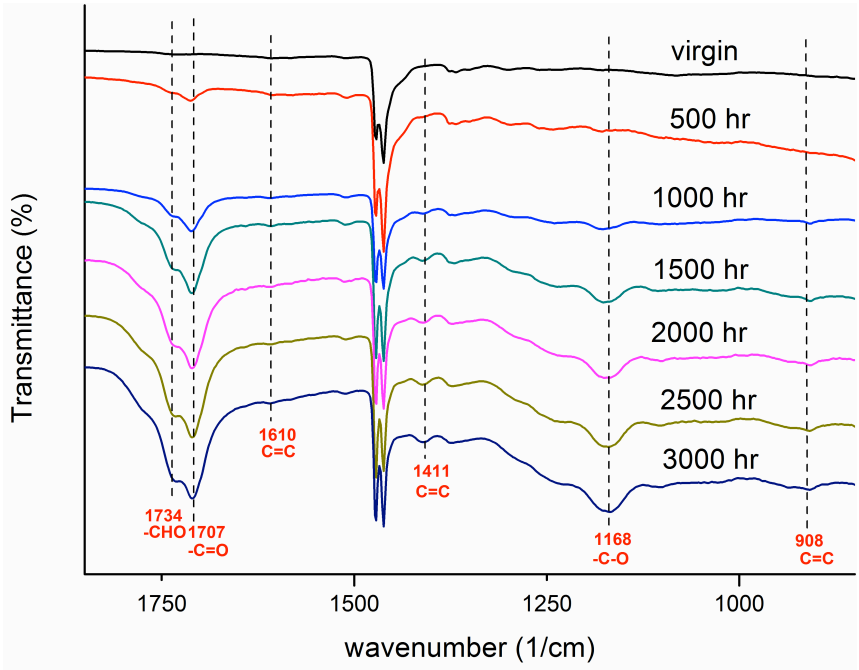

Fig. 42. FTIR spectra of Sample T after different lengths of UV irradiation

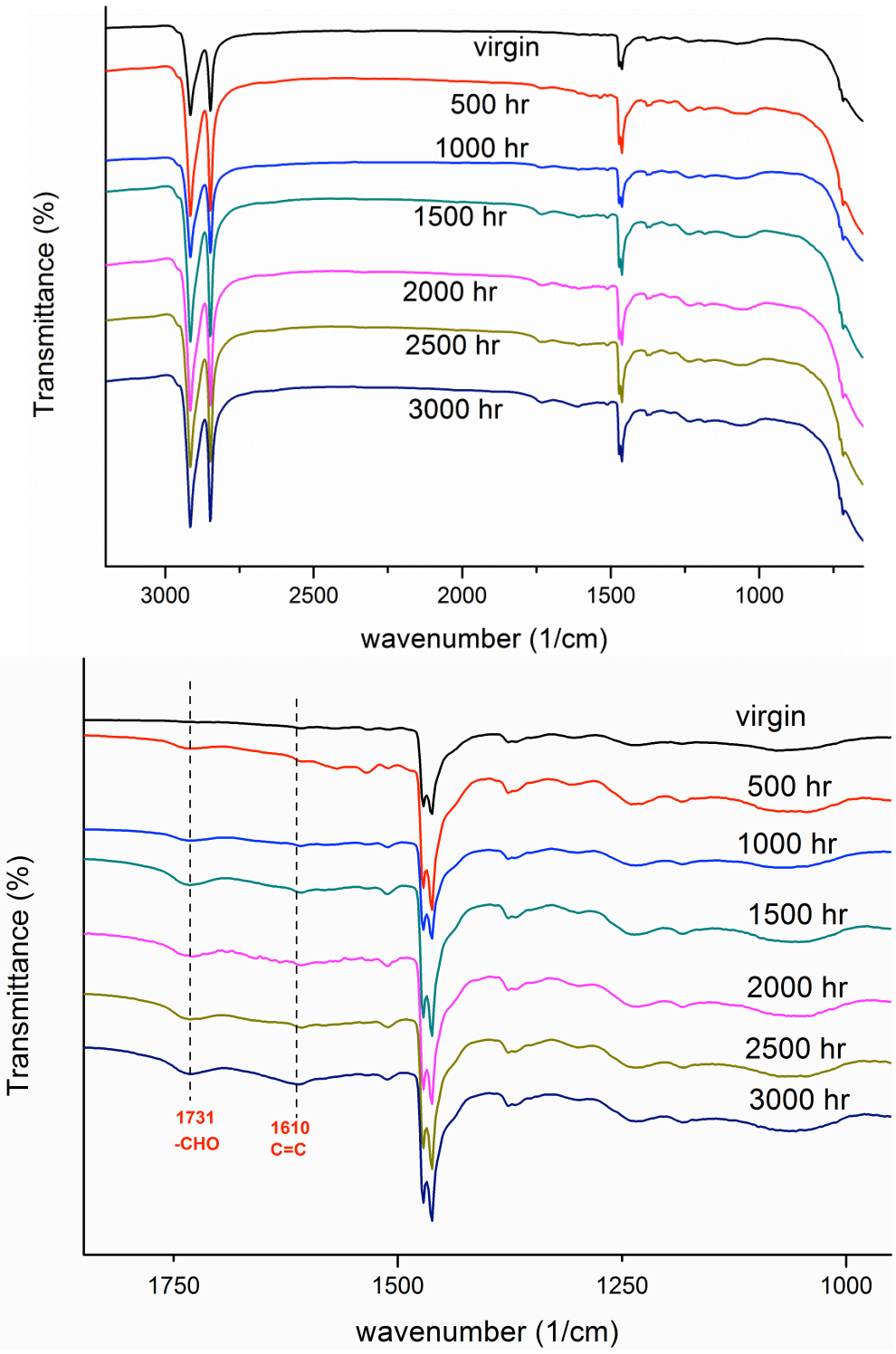

Fig. 43. FTIR spectra of Sample K after different lengths of UV irradiation

Samples C and M2 show peaks at 1740 cm^{-1} (C=O stretching of -COO-) and at 1239 and 1019 cm^{-1} (C-O stretching of -COO-), which are characteristic peaks of EVA.[76] The two samples share very similar trend of spectrum change. Peak 1740 cm^{-1} is strengthened and broadened with increasing irradiation time, suggesting the formation of more carbonyl bonds during EVA degradation. The occurrence and strengthening of 1710 cm^{-1} peak (C=O stretch in acids) is due to the increasing content of the degradation product of acetic acid.[64] The Peaks at 1239 and 1019 cm^{-1} decrease in intensity, indicating the decreasing content of the original ester groups of EVA due to the release of acetic acid during degradation. The occurrence of the peak around 1163 cm^{-1} suggests the formation of oxidation induced new -COO- groups, which are different from the ones in original EVA.[76] The peaks around 1412 cm^{-1} are attributed to carbon double bonds (-C=C-), which are also the products of oxidation.[76]

The surface layer of samples T and sample K is made of low-density polyethylene (LDPE). Their FTIR spectra feature peaks of $–CH_2-$ backbone. For sample T, the increasing intensity of the 1734 and 1707 cm^{-1} peaks is attributed to C=O stretches from ester and ketone groups produced by LDPE oxidation.[52,53] The peaks at 1610, 1411, and 908 cm^{-1} show that carbon double bonds (C=C) are formed in the aging process.[44] The peak at 1168 cm^{-1} is attributed to C-O stretch in alcohols that are produced from LDPE photooxidation.[54] For sample K, only weak peaks at 1731 (C=O) and 1610 (C=C) cm^{-1} can be noticed, suggesting minimal degradation of the sample. These results are in good agreement with those from visual, SEM, and color studies, i.e., sample K exhibits the best UV degradation performance.

4.7. Dielectric Properties

In addition to its mechanical protection and optical reflection functions, another major function of polymeric backsheets is electric insulation. Electrical resistivities and permittivities of the samples at 1000 Hz is shown in Fig. 44. The resistivities and permittivities of all the samples are close and remain relatively constant despite increasing irradiation time. These results do not show the trends that have been observed in YI, Delta E, microstructure, and FTIR studies. This is because the electrical test includes all the layers in the backsheets while only the top layer is tested in the previous tests. In general, the results show that all backsheets possess good electrical insulation property which is only slightly affected by UV aging. The safety risk of electric shock/leak due to UV aging can be largely eliminated.

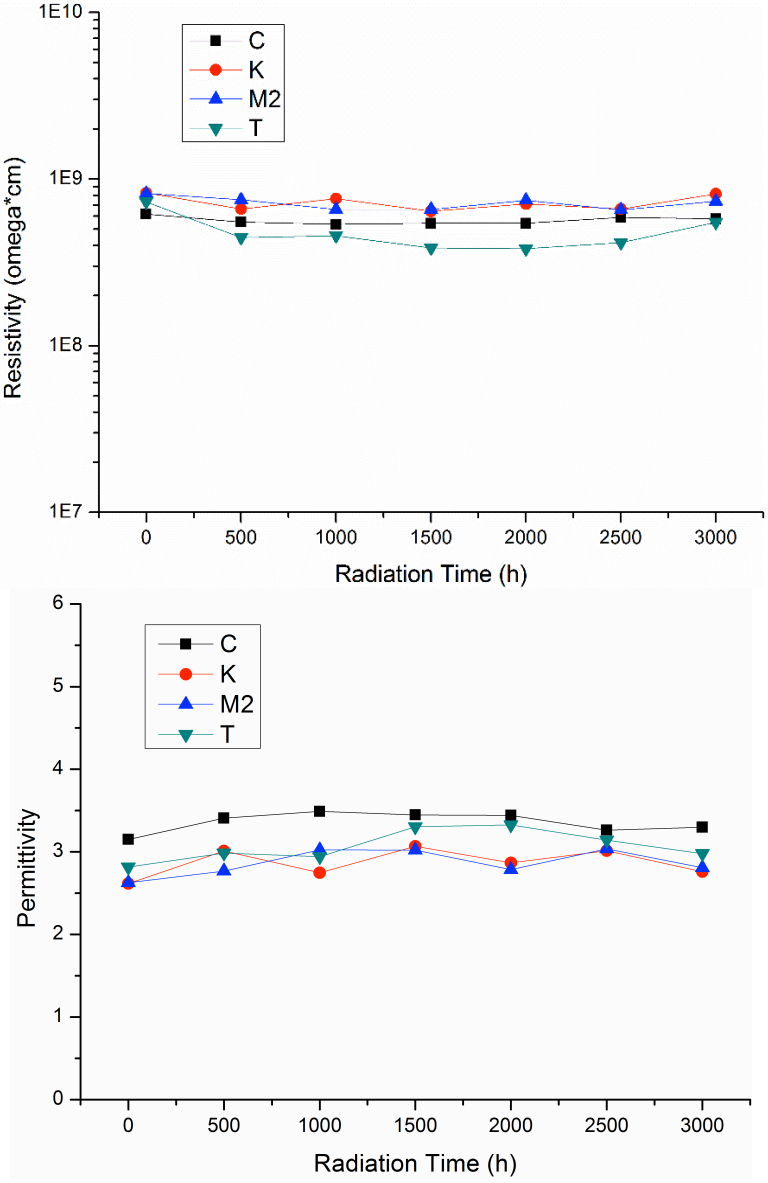

Fig. 44. Resistivity and permittivity of the samples at a frequency of 1000 Hz

CHAPTER 5. CONCLUSIONS

UV aging tests on four different commercial PV polymeric backsheets were performed. Systematic optical, microstructural, chemical, and electrical analyses were conducted on the aged samples after different hours of UV aging. Optical microscopy and SEM studies showed that sample surface cracking and interlayer delamination developed with increasing irradiation dosage. Sample residual stresses played an important role in crack propagation.

A linear relationship between YI and UV irradiation dosage was established, which can be used to predict longer term yellowing behavior of the materials. YI was found to be equivalent to Delta E in measuring sample color change after UV exposure. Different labs and researchers can compare their results even though they are using different parameters. Surface reflection of the backsheets decreased with increasing UV dosage, which was in agreement with the results from YI.

Underlying degradation mechanisms were studied using FTIR and the degradation products were identified. The degree of degradation was related to the progress of yellowing. UV degradation of the backsheets did not influence their electrical properties within the tested irradiation time because degradation only occurred on the sample surfaces. The effects are expected to show under very large UV dosages.

All the backsheets tested in this research are qualified commercial products. However, one of the four backsheets showed severe premature UV degradation and hence its use in commercial PV modules might cause PV quality issues after a certain period of time of UV exposure. This study highlighted the importance of material evaluation for the PV industry.

For 25 years of lifetime warranty, PV module manufacturers need to exercise due diligence to qualify the right material into their product.

The results have also provided the PV QA task force much needed information to develop proper UV aging standards for the PV industry. Future work of this study is to continue the UV aging study on the same material under other three light/UV conditions: metal halide, Xenon arc, and EMMAQUA (~5X concentrated natural sunlight), and to correlate the results to establish systematic relationships between the aging conditions and the aging results for the materials under study. In addition, more work is needed to correlate the accelerated testing results to field failures.

President Obama urged extensive use of renewable energy in his inaugural address in January 20th, 2009 - "We will harness the sun and the winds and the soil to fuel our cars and run our factories."[77] Reliable PV technology is crucial to the success of solar energy, which highlights the importance of the studies on the aging behaviors of PV backsheets.

REFERENCES

(1) Markvart, T. *Solar electricity. 2nd edition*; John Wiley & Sons, 2000.
(2) Swanson, R. M. *Science (80-.)*. **2009**, *324*, 891–892.
(3) Chapin, D. M.; Fuller, C. S.; Pearson, G. L. *J. Appl. Phys.* **1954**, *25*, 676.
(4) Murphy, T. Don't Be a PV Efficiency Snob http://physics.ucsd.edu/do-the-math/2011/09/dont-be-a-pv-efficiency-snob/.
(5) Messenger, R.; Ventre, J. *Photovoltaic systems engineering*; 2003.
(6) Photovoltaic Electrical Contacts and Cell Coatings http://www.eere.energy.gov/basics/renewable_energy/pv_contacts_coatings.html.
(7) How PV Cells Are Made http://www.solala.eu/cms/?Photovoltaic_Technology:How_PV_Cells_Are_Made.
(8) Curtis, R. What is solar power? http://www.mrsolar.com/content/what-is-solar-power.php.
(9) Best research-cell efficiencies http://www.nrel.gov/ncpv/images/efficiency_chart.jpg.
(10) Yang, S.; Whitfield, K. Thermal Endurance Study of Polymers Used in LCPV.
(11) Zipp, K. Solar thin films provide a path to grid parity http://www.solarpowerworldonline.com/2011/04/solar-thin-films-provide-a-path-to-grid-parity/.
(12) Pern, J. *Module Encapsulation Materials, Processing and Testing*; Shanghai, China, 2008.
(13) Osterwald, C. R.; Mcmahon, T. J. *Prog. Photovoltaics Res. Appl.* **2009**, *17*, 11–33.
(14) Yang, S. Private communication with Shuying Yang,03/11/2013.
(15) Yang, S. .
(16) Fire risk fiasco as Dutch government warns over 650,000 Scheuten Solar modules http://www.pv-tech.org/news/fire_risk_fiasco_as_dutch_government_warns_about_650000_scheuten_solar_modu.
(17) Koehl, M. In *2nd International PV Module Quality Assurance Forum*; 2011.
(18) Why Do Backsheets Matter? http://www.honeywell-powershield.com/backsheet-importance/#backsheet-importance.
(19) International PV Module Quality Assurance Task Force http://www.nrel.gov/ce/ipvmqa_task_force/.
(20) *Crystalline silicon terrestrial photovoltaic (PV) modules – Design qualification and type approval*; 2005.
(21) *Photovoltaic (PV) module safety qualification - Part 1: Requirements for construction*; 2013.
(22) *Standard for Flat-Plate Photovoltaic Modules and Panels*; 2002.
(23) *Concentrator Photovoltaic Modules and Assemblies*.
(24) *Thin-film terrestrial photovoltaic (PV) modules - Design qualification and type approval*; 2008.

(25) Koehl, M.; Philipp, D.; Lenck, N.; Zundel, M. *Development and Application of a UV Light Source for PV-Module Testing*; Golden, Colorado, 2012.
(26) Dunn, L.; Gostein, M.; Stueve, B. *Literature Review of the Effects of UV Exposure on PV Modules*; Austin, Texas, 2013.
(27) EMMAQUA http://atlas-mts.com/services/natural-weathering-testing-services/accelerated-weathering/emmaqua/ (accessed Nov 22, 2013).
(28) Light Engines for the Life Sciences http://www.americanlaboratory.com/913-Technical-Articles/18653-Light-Engines-for-the-Life-Sciences/.
(29) SPECTRA OF FLUORESCENT LIGHT BULBS http://ledmuseum.candlepower.us/led/spectra7.htm.
(30) Cinema Lamps - reliability starts here http://www.christiedigital.co.uk/emea/cinema/cinema-products/cinema-lamps/Pages/default.aspx.
(31) Yang, S. Private communication with Shuying Yang,10/30/2013.
(32) ASTM E313-00 Standard Practice for Calculating Yellowness and Whiteness Indices from Instrumentally Measured Color Coordinates **2001**.
(33) Kempe, M. D.; Moricone, T. J.; Kilkenny, M. **2011**.
(34) Protekt® http://www.madico.com/pv-backsheets/product/protekt/.
(35) Oreski, G.; Wallner, G. M. *Sol. Energy* **2005**, *79*, 612–617.
(36) Densley, R. J.; Bartnikas, R.; Bernstein, B. *IEEE Trans. Power Deliv.* **1994**, *9*, 559–571.
(37) Ciuprina, F.; Teissèdre, G.; Filippini, J. C. *Polymer (Guildf).* **2001**, *42*, 7841–7846.
(38) McLaughlin, W. L.; Silverman, J.; Al-Sheikhly, M.; Chappas, W. J.; Zhan-Jun, L.; Miller, A.; Batsberg-Pedersen, W. *Radiat. Phys. Chem.* **1999**, *56*, 503–508.
(39) Allen, N. S.; Edge, M.; Holdsworth, D.; Rahman, A.; Catalina, F.; Fontan, E.; Escalona, A. M.; Sibon, F. F. *Polym. Degrad. Stab.* **2000**, *67*, 57–67.
(40) Wu, Q.; Qu, B.; Xu, Y.; Wu, Q. *Polym. Degrad. Stab.* **2000**, *68*, 97–102.
(41) Gulmine, J. V.; Akcelrud, L. *Polym. Test.* **2006**, *25*, 932–942.
(42) Lee, A. W.; Santerre, J. P.; Boynton, E. *Biomaterials* **2000**, *21*, 851–861.
(43) Haider, N.; Karlsson, S. *Polym. Degrad. Stab.* **1999**, *64*, 321–328.
(44) Gugumus, F. *Die Angew. Makromol. Chemie* **1990**, *182*, 111–134.
(45) Gugumus, F. *Polym. Degrad. Stab.* **2000**, *68*, 337–352.
(46) Gugumus, F. *Polym. Degrad. Stab.* **2002**, *76*, 95–110.
(47) Gugumus, F. *Polym. Degrad. Stab.* **2002**, *75*, 55–71.
(48) Gugumus, F. *Polym. Degrad. Stab.* **2001**, *74*, 327–339.
(49) Gugumus, F. *Polym. Degrad. Stab.* **2002**, *76*, 381–391.
(50) Gugumus, F. *Polym. Degrad. Stab.* **2002**, *75*, 131–142.
(51) Khabbaz, F.; Albertsson, A.-C.; Karlsson, S. *Polym. Degrad. Stab.* **1998**, *61*, 329–342.
(52) Gugumus, F. *Polym. Degrad. Stab.* **1999**, *65*, 5–13.
(53) Lacoste, J.; Carlsson, D. J.; Falicki, S.; Wiles, D. . *Polym. Degrad. Stab.* **1991**, *34*, 309–323.
(54) Gijsman, P.; Meijers, G.; Vitarelli, G. *Polym. Degrad. Stab.* **1999**, *65*, 433–441.
(55) Koenig, J. L.; Boerio, F. J.; Plueddemann, E. P.; Miller, J.; Willis, P. B.; Cuddihy, E. F. *Chemical bonding technology: Direct investigation of interfacial bonds*; 1986.
(56) Hoelscher, J. F. *15th Photovolt. Spec. Conf.* **1981**, *1*, 745–749.

(57) Cuddihy, E. **1982**.
(58) Cuddihy, E. F.; Coulbert, C. D.; Liang, R. H.; Gupta, A.; Willis, P.; Baum, B. *NASA STI/Recon Tech. Rep. N* **1983**, *83*, 29809.
(59) Claassen, R. S.; Butler, B. L. *Sol. Mater. Sci.* **1980**, *1*, 3–51.
(60) Pern, F. J. *Die Angew. Makromol. Chemie* **1997**, *252*, 195–216.
(61) Wenger, H. J.; Schaefer, J.; Rosenthal, A.; Hammond, B.; Schlueter, L. In *The Conference Record of the Twenty-Second IEEE Photovoltaic Specialists Conference - 1991*; IEEE: Las Vegas, NV, 1991; pp. 586–592.
(62) Jordan, D. C.; Kurtz, S. R. *Prog. Photovoltaics Res. Appl.* **2013**, *21*, 12–29.
(63) Kempe, M. D.; Jorgensen, G. J.; Terwilliger, K. M.; Mcmahon, T. J.; Kennedy, C. E. **2006**.
(64) Costache, M. C.; Jiang, D. D.; Wilkie, C. A. *Polymer (Guildf).* **2005**, *46*, 6947–6958.
(65) Czanderna, A. W.; Pern, F. J. *Sol. Energy Mater. Sol. Cells* **1996**, *43*, 101–181.
(66) Griffiths, P. R.; Haseth, J. A. de *Fourier Transform Infrared Spectrometry*; 2nd ed.; Hoboken, New Jersey, 2007; p. 560.
(67) *Clin. Sci.* **1957**, *16*.
(68) *Polymeric Materials – Use in Electrical Equipment Evaluations*; 2010.
(69) *ASTM G26-96 Practice for Operating Light-Exposure Apparatus (Xenon-Arc Type) With and Without Water for Exposure of Nonmetallic Materials*; 1996.
(70) QUV Accelerated Weathering Tester http://www.q-lab.com/products/quv-weathering-tester/quv (accessed Nov 26, 2013).
(71) *Fraunhofer ISE CalLab PV Cells changes to new spectral distribution in IEC 60904-3 standard*.
(72) *Weathering 101 The Basics of Weathering & Light Stability*.
(73) Daro, A.; Trojan, M.; Jacobs, R.; David, C. *Eur. Polym. J.* **1990**, *26*, 47–52.
(74) Color difference - Wikipedia, the free encyclopedia http://en.wikipedia.org/wiki/Color_difference.
(75) Sharma, G.; Bala, R. *Digital Color Imaging Handbook*; CRC Press, 2010; p. 816.
(76) Lin, V.; Colthup, N.; Fateley, W.; Grasselli, J. *The handbook of infrared and raman characteristic frequencies of organic molecules*; Academy Express: San Diego, 1991; p. 503.
(77) Transcript - Barack Obama's Inaugural Address - Text - NYTimes.com http://www.nytimes.com/2009/01/20/us/politics/20text-obama.html?pagewanted=all (accessed Jul 22, 2013).